Control Systems Approach to Balance Stabilization during Human Standing and Walking

by

Amy R. Wu

A dissertation submitted in partial fulfillment
of the requirements for the degree of
Doctor of Philosophy
(Mechanical Engineering)
in the University of Michigan
2015

Doctoral Committee:

Professor Arthur D. Kuo, Chair
Professor Daniel P. Ferris
Associate Professor Brent Gillespie
Associate Professor Kathleen H. Sienko

To Pluto. What it was and is no longer, if only temporarily categorized by meager human minds within the context of the unfathomable expanse of space.

On January 19, 2006, I stood at Cape Canaveral watching my first ever launch, an Atlas V rocket carrying NASA's New Horizons spacecraft. We were told it would take 9 years to reach Pluto, then the 9th planet of our solar system. We tried to predict the future and now it has arrived.

A C K N O W L E D G M E N T S

One, unless superhuman, cannot go through graduate school without support from family, friends, and a great academic community.

First and foremost, I would like to thank Art Kuo for his invaluable insight, mentorship, and for creating a lab environment that is both scientifically interesting and a lot of fun! I can never introduce a topic now without thinking how saving Princess Leia could apply. I am also grateful for my committee: Dan Ferris, Kathleen Sienko, and Brent Gillespie for all their great advice and guidance throughout the years. I would like to thank their labs and other members of the neuromechanics community (David Remy, Deanna Gates) for all the interesting discussions and feedback. I especially would like to thank members of HBCL for all the help, advice, and for being a great support network.

I am grateful for the National Defense Science and Engineering (NDSEG) program for providing funding for three years.

I would also like to acknowledge Eli Livne at the University of Washington, whom inspired me to start my academic career. When I later became disillusioned with graduate school, his support was instrumental in keeping me going. I would also like to thank Michael O'Grady at Boeing. There are many bosses in the world but very few leaders. I am grateful for his support of my continued education.

To my friends! Thank you to the members of the House of Destruction- Asad, Kenny, Gerardo, Alexey, and Matt. Whether we are trying to finish a pset in the Duderstadt or driving down to the Red, thank you so much for all the good times. Thank you to Sasha for the climbs, runs, and coffee breaks, where we talked about research of course.

Finally, I would like to thank my family for their support. To my dad Ru for all his wonderful advice, my mom Sue for trying to keep me healthy and hydrated, and to my brother Terry for being awesome. To my husband Matt Robertson, who has been there from the very beginning. Thank you for all your crazy ideas, for grounding me, and for being my home.

TABLE OF CONTENTS

LIST OF FIGURES

LIST OF TABLES

ABSTRACT

Control Systems Approach to Balance Stabilization during Human Standing and Walking

by

Amy R. Wu

Chair: Arthur D. Kuo

Humans rely on cooperation from multiple sensorimotor processes to navigate a complex world. Poor function of one or more components can lead to reduced mobility or increased risk of falls, particularly with age. At present, quantification and characterization of poor postural control typically focus on single sensors rather than the ensemble and lack methods to consider the overall function of sensors, body dynamics, and actuators. To address this gap, I propose a controls framework based on simple mechanistic models to characterize and understand normative postural behavior. The models employ a minimal set of components that typify human behavior and make quantitative predictions to be tested against human data.

This framework is applied to four topics relevant to daily living: sensory integration for standing balance, limb coordination for one-legged balance, momentum usage in sit-to-stand maneuvers, and the energetic trade-offs of foot-to-ground clearance while walking. First, I demonstrate that integration of information from multiple physiological sensors can be modeled by an optimal state estimator. Second, I show that feedback control can model multi-limb coordination strategies during one-legged balance. Third, I use optimization models to demonstrate that momentum usage in sit-to-stand maneuvers employs excess work but serves to balance effort between knee and hip. Fourth, I propose a model for preferred ground clearance during swing phase of walking as a cost tradeoff between inadvertent ground contact and foot lifting, modulated by movement variability. These controls-based models demonstrate the mechanisms behind normative behavior and enables predictions under novel situations. Thus these models may serve as diagnostic tools to identify poor postural control or aid design of intervention procedures.

CHAPTER 1

Introduction

Humans rely on cooperation from multiple sensorimotor processes to navigate a complex world. Control of body dynamics, appropriate movement strategies, and resolution of conflicting sensory information are necessary to tolerate environmental challenges [28]. Poor function of one or more components can lead to poor mobility or increased risk of falls, particularly with age. At present, quantification and characterization of poor postural control typically focus on single sensors rather than the ensemble and lack methods to consider the overall function of sensors, body dynamics, and actuators. To address this gap, I propose a controls framework based on simple mechanistic models to characterize and understand the normative postural behavior. This framework is applied to four topics relevant to daily living: sensory integration for standing balance, limb coordination for one-legged balance, momentum usage in sit-to-stand maneuvers, and the energetic trade-offs of foot-to-ground clearance while walking.

We model balance and coordination with controls theory because humans are dynamical systems that rely on appropriate body responses to environmental disturbances (feedback control) and proper apportion of muscles for preset movements (feedforward control). For example, balance on one leg requires feedback control from limbs to stabilize the center of mass (COM) against spontaneous fluctuations. The sit-to-stand maneuver demonstrates feedforward control, where a predetermined set of muscle activations coordinate knee and hip motion. Controllers can also be optimal when derived from minimizing some cost function. In foot clearance, the controlled height weighs risk of tripping against cost of leg lift. The mathematical dual of a feedback controller is a state estimator, which reconstructs observable states of interest from available measurements. State estimators could be used to model how the central nervous system integrates sensory measurements to produce an estimate of body position. The controls approach has been used to model postural control of upright standing [44,46], sensory integration [9,40,54], and optimal control of muscular movements [2,50,64]. The models range from single inverted pendulums to multi-degree of freedom, musculoskeletal systems. We use an intermediate degree of complexity with a

minimal set of essential components that typify human behavior. Furthermore, we employ established mathematical methods from controls theory to generate predictions testable against human data.

In the first chapter, I examine how the central nervous system (CNS) may resolve conflicting sensory information. Postural responses are driven by multiple sensory modalities, each of which has its own dynamics. Sensory measurements from vision, the vestibular system, and proprioception can conflict, and resolution of this incompatibility by the central nervous system can manifest in postural response. For instance, the tilt response of a quietly standing individual to a constant velocity, roll-axis optokinetic stimulus is to lean with slow dynamics in the direction of the optic flow without falling over [36]. Many studies have quantified the transient and steady-state effect of visual perturbations on postural behavior [36,47,65]. However, few have provided an explanation or model for how the resolution of conflicting information would produce such a postural response. One proposed model characterized the effect of visual perturbations on the ankle joint, but the vestibular organs and proprioceptors were modeled as noise, suggesting those dynamics were unimportant to the postural response [67]. Another model accounted for sensor dynamics in an estimator model to explain postural responses to constant yaw rotations and lateral accelerations [9]. However, this model did not include roll-axis tilt perturbations. Hence, there is no model that comprises multiple sensor dynamics and predicts tilt response to roll vection. Here we propose that information is combined optimally using an internal model of the body and sensor dynamics and subject to some noise characteristics, similar to Borah's model. However, we develop a simpler model with the minimal number of parameters sufficient enough to explain the roll-axis tilt behavior. In particular, we believe the initial lean arises from canals dynamics and the saturation emerges from a compromise of all sensor measurements.

In the second chapter, a similar controls model is employed to study one-legged lateral balance strategies. Humans employ a variety of strategies for balance control, including center of pressure (COP), angular momentum, or an external force [27,63]. These methods help regulate the body center of mass (COM) within the base of support (BOS). Balancing on one leg, however, presents a unique challenge, in part because the stance foot can only exert limited torques on the ground. Balance therefore depends much more on motion of the other limbs, which can move the body center of mass (COM) only indirectly [48]. While many can perform such one-legged balance with ease, few models have considered how multiple limbs should be coordinated and in what ways to keep the body stabilized. Therefore, we propose a simple balance model based on angular momentum principles to explain limb coordination and compare model predictions to human behavior. In addition,

environmental conditions may make that strategy infeasible, for example, when the base of support is reduced in size. How is the nominal coordination strategy altered to enable balance feasible? We propose that compensatory limb movements, such as increased contributions from free limbs, are required to balance under those constraints.

The controls models of the previous two chapters can be generalized as an optimization to minimize some cost function. In the third chapter, I investigate the effect of minimizing work and other cost functions for a sit-to-stand movement. Many human motions are performed with energetic economy, which depend on mechanical work and other aspects of muscular effort. For a sit-to-stand (STS) movement, the theoretical minimum required for mechanical work is the gravitational potential energy gained between the two positions. An economic motion might approach this minimum if negative work could be avoided. Older adults, for example, favor a strategy that repositions their center of mass (COM) closer to their base of support (BOS) prior to seat-off [30, 59, 61]. This avoids momentum usage and thereby employs minimal work. In contrast, young healthy adults commonly use initial trunk momentum to aid in rising [34, 49, 56]. This entails negative work as the hips extend against the trunk's forward momentum and therefore requires more positive work to stand. Consequently, younger adults would appear to spend more energy than older adults to stand. This is surprising because younger adults are typically the benchmark for comparison against the elderly and thus expected to exhibit behavior that optimizes energy expenditure. To ascertain if there is an advantage to using momentum from sit-to-stand, we employ a simple chair rise model and test whether momentum usage requires excess work. We also determine what benefits the strategy might offer over other strategies that may be more stabilizing, requires little joint coordination, or avoids actuating particular joints. Previous models have also suggested that minimizing torque derivative cost is an important criterion to mimicking chair rise [49]. Therefore, we also include a torque time-derivative cost, in addition to work, and propose that some combination of both could reproduce important components of chair rise behaviors.

Control of foot clearance to the ground is an important aspect of fall avoidance and inability to provide adequate clearance may increase fall risk. Older adults have been found to walk with reduced knee flexion and ankle dorsiflexion during the swing phase compared against young subjects, reducing ground clearance [5]. In addition, greater foot clearance variability has been shown in older adults compared to younger adults and in older fallers compared to older non-fallers [3]. Statistical models have been developed to capture key parameters of the probabilistic distribution of clearance to determine trip avoidance strategies [4]. Those clearance histograms of elderly subjects, for example, show reduced median height when compared against young subjects, which indicates a preference for

decreasing energetic cost of gait at the expense of increased tripping risk. The clearance probability distribution suggests the existence of a preferred clearance height and alludes to a tradeoff between energetic cost of leg lift and risk of tripping. However, no proof exists for this commonly held assumption. Since much of gait seems to be energetically optimal, we use metabolic cost to compare walking at different foot clearance heights. We use scuffing as a proxy for negative leg lift. We expect that the preferred clearance height minimizes metabolic cost. We hypothesize that greater leg lifting decrease likelihood of tripping but should require more work. Greater scuffing should also require more work due to drag force on the ground. We propose that the expected cost of ground clearance includes the cost of scuffing and cost of leg lift and is modulated by uncertainty in clearance movements.

CHAPTER 2

Sensory integration model of postural response to lateral visual perturbations.

2.1 Introduction

Humans control postural balance through sensory modalities including vision, vestibular organs, and somatosensors. Each modality has distinctive dynamics—sensitive to a particular frequency range and type of motion—that must be integrated by the central nervous system (CNS) to indicate the body's state. Such integration is evidenced by the body's response to conflicting or illusory sensory inputs. A long-observed example is the optokinetic roll response, where a standing human, surrounded by a visual field rotating about the roll axis at constant angular speed, will tilt their body in the same direction as the field [36, 65]. The response is not immediate but gradually builds over several seconds following stimulus onset [36, 65], similar to a low-pass filter [25]. The timing is considerably slower than the response time of the visual system, and therefore appears to be attributable to CNS processing downstream of vision. The person also usually does not fall over [75], indicating that other posture sensors are integrated and help counteract the visual stimulus. However it is unknown why the CNS should react so slowly, given that many postural responses must occur within a second or so to avoid falling. An explanation for the postural response to optokinetic roll stimulus might yield insight on how the CNS integrates information for posture control.

The optokinetic roll response can be reproduced by a relatively simple model with a shared neural time-integrator [25]. Visual, vestibular, and body tilt sensory data are linearly combined with individual weights, and then fed through a single shared integrator, which effectively acts as a filter of sensory information. With appropriate configuration of weightings between sensors, such a model can reproduce the basic postural responses to the optokinetic stimulus. It can also reproduce responses to artificial vestibular stimulus where direct current galvanic stimulus is applied to the mastoid processes, producing a

transient response more similar to a high-pass filter. This is somewhat reminiscent of the shared "velocity storage" integrator observed in visual-vestibular interactions governing spatial self-orientation [12, 57, 58]. An optokinetic stimulus about the yaw (vertical) axis is interpreted by a seated person as continuous self-motion, also with low-pass filter characteristics. A corresponding vestibular stimulus about vertical also induces self-motion, albeit as a high-pass filter. The two paradigms are analogous, except that the roll-axis postural tilt response is one of angular displacement, whereas the yaw-axis self-motion illusion is of angular velocity.

The shared integrator model does not, however, explain why a neural integrator or any kind of filtering might be useful for posture. An alternative approach is to consider how the CNS might optimally detect its state without presuming a particular filter. An optimal state estimator (see Fig. 2.1) uses an internal model to predict the output of multiple, noisy sensors and yield an estimate of body state with minimum mean-square error [11], through feedback to correct the mismatch between actual and expected afference. Such models have long been proposed for both visual-vestibular interactions (e.g. [9, 24]) and posture (e.g. [37, 38, 40, 68]), along with physiological explanations for how the cerebellum could mediate adaptation of the CNS internal model [52, 53]. However these models tend to be quite complex, making it unclear whether their behaviors are compatible with the relatively simple postural responses to optokinetic roll stimulus.

Given the mismatch between model complexity and the prior experimental data, a concern arises whether a complex model can in fact explain a simple experiment. In the case of self-orientation, a relatively complex model of three-dimensional head rotations, subject to visual and vestibular perturbations, can indeed reproduce simple experimental observations, for example single-axis optokinetic responses and vestibular responses, such as an illusion of self-motion following the end of a sustained head rotation (e.g., post-rotatory responses and optokinetic afternystagmus; [9]). In the case of posture control, the resolution is less clear. This is due in part to the greater number of degrees of freedom in the body than the head alone, and to the greater challenge of experimentally perturbing these degrees of freedom and the greater number of sensory modalities associated with them. It is also not straightforward to interpret how the sophisticated models reported in the literature would respond within a classic experimental paradigm. However given the success of models for visual-vestibular interactions, the conceptually similar posture control models might perform similarly well.

The purpose of the present study is to test a state estimation model for posture against the classic optokinetic stimulus. We first analyze a state estimation model to determine whether it predicts response similar to the low-pass filter behavior of the shared neural

integrator model (eg. [25]). We then experimentally apply optokinetic perturbations to standing humans and test whether their behavior is compatible with the expected low-pass filter description (Figure 2.1). Rather than apply the traditional step in angular velocity for the stimulus, we instead apply a series of sinusoidal stimuli over a range of frequencies. If the CNS behaves like a dynamic system, the same low-pass filter can be predicted and tested in the frequency domain as well as the time domain (sinusoidal response vs. step response, respectively). The low-pass filter thus serves as a bridge between a complex state estimator model and a relatively simple experiment. We thus hope to resolve whether state estimation theory applies as well to posture control as it does to visual-vestibular interactions.

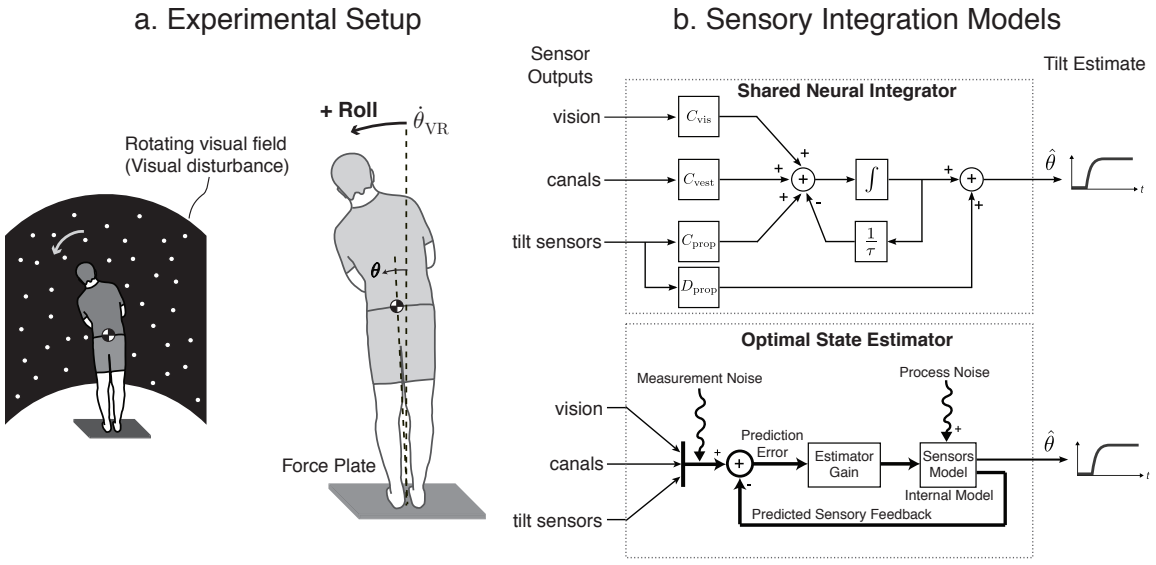

Figure 2.1: Roll vection in upright standing, and two proposed models for sensory integration. (a) Subjects were visually perturbed by sinusoidal rotations in the roll direction (left), and their tilt response θ recorded (right), defined as the center of pressure excursion in the mediolateral direction divided by leg length. (b) Shared neural integrator model (top) reproduces observed responses through sensory weightings and a shared time constant τ to combine sensory measurements. The estimator model (bottom) derives tilt estimate $\hat{\theta}$ by minimizing the error between measured tilt and estimated tilt (bottom). Both models' $\hat{\theta}$ capture tilt response θ to a step in visual disturbance.

2.2 Sensory Integration Model

We model sensory integration for posture with a simple optimal estimator and test whether the model reproduces low-pass filter behavior to visual perturbations, as previ-

ously observed in [25]. We use a linear model of roll-axis behavior, including minimal sensor dynamics sufficient to capture the visual-vestibular interaction (Figure 2.2). The sensor models respond to angular velocity input $\dot{\theta}$. Vision may also be perturbed by optokinetic stimulus $\dot{\theta}_{\text{VR}}$. The estimator is derived from sensor dynamics, and with sensory channels as inputs, the model produces an estimate of body tilt $\hat{\theta}$ as output (Figure 2.2).

We model sensors with simple, first-order dynamics, which were previously reported and used for the neural integrator [25]. Vision can measure angular velocity of self-motion relative to the environment [58]. The canals act as a high-pass filter with dynamics dominated by the cupula time constant T_{c} [19]. The time constant T_{c} is approximately 7 seconds for humans [58]. We include a general tilt sensor that aggregates multiple sensors whose dynamics we consider to be fast relative to the optokinetic response. This include the otoliths, which provide an indication of tilt through acceleration of gravity, as well as proprioception, which, dominated by muscle spindles, measure joint angles through sensing changes in muscle length [33]. The tilt sensor model measures body angle with the integral of the angular velocity input. The dynamic sensor models can predict the sensory output to any angular velocity input. If a step in angular velocity were applied to this system, the sensors model's response would be a step signal in angular velocity for vision, a high-pass filtered response for the canals, and a ramp in angles for the tilt sensors.

The sensor outputs are fed into the state estimator model of sensory integration. The state estimator has two key components (Figure 2.1), an internal model of the body and sensors, and a feedback of prediction error through an estimator gain (see Appendix for details). That gain is determined by uncertainty in the system, modeled as zero-mean sensor noise and process noise, both characterized by covariance matrices. Sensor measurement noise accounts for imperfect or corrupted sensors, and process noise accounts for unknown disturbances and internal model uncertainty. There is one variance value for process noise, and the three sensors are treated as independent and having three variance values. Thus with sufficient sensor measurements, noise variances, and internal model accuracy, tilt estimate $\hat{\theta}$ converges to actual tilt.

We approximate measured tilt response θ by estimated tilt $\hat{\theta}$. The body controller can use the estimated tilt $\hat{\theta}$ to execute corrective body movements, for example. However, based on frequency analysis of voluntary oscillations from human subjects, the bandwidth for human body dynamics is 3.41 rad/s. This is equivalent to a time constant of 0.29 s, much faster than the slow dynamics (7 s) of the semicircular canals. Hence, we treat the controller as fast relative to the canals.

The estimator model predicts the effects of sensory perturbations, including visual disturbances. The transfer function from visual disturbance to tilt output yields a second-order

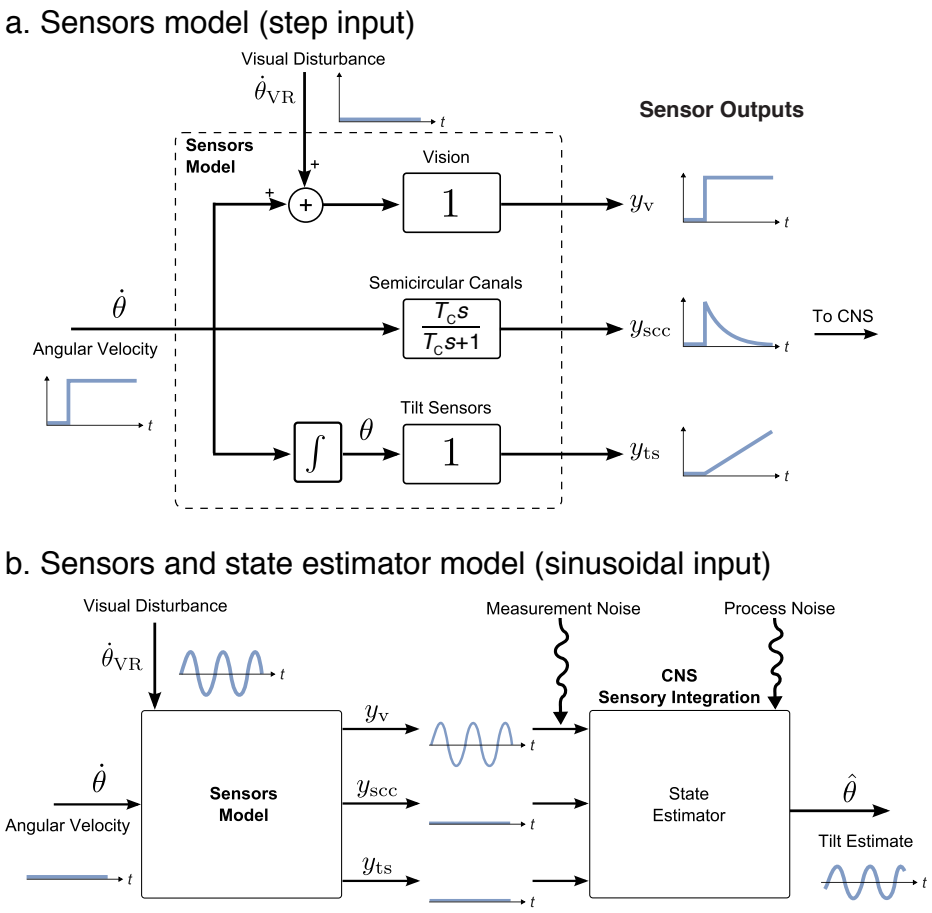

Figure 2.2: Sensors and state estimator model block diagrams. (a) Vision measures the angular velocity input, the semicircular canals act as a high-pass filter with cupula time constant T_c, and the tilt sensors are modeled as an integrator, all represented as transfer functions with s as complex frequency (rad/s) of the Laplace transform. The response to a step input in the body's angular velocity is a sustained step in vision, a decaying exponential in canals, and a ramp response in tilt sensors. (b) To a sinusoidal visual disturbance, the vision output is the only non-zero sinusoidal response. This response is fed into the state estimator, whose tilt estimate $\hat{\theta}$ is governed by sensor dynamics and uncertainties in the form of measurement noise and process noise. For a linear system, a sinusoidal visual disturbance $\dot{\theta}_{VR}$ produces a sinusoidal tilt with amplitude and phase that varies with frequency.

system, which we compare with the first-order, low-pass filter dynamics of the shared neural integrator (Figure 2.3a). Indeed, the estimator is found to exhibit first-order, low-pass behavior. In the time domain, its response to a step input is sustained at some constant, instead of decaying to zero, and the initial rise of its response can be approximated by one exponential. In the frequency domain, the magnitude and phase delay decreases as the visual disturbance frequency increases, suggesting low-pass behavior (Figure 2.3b). In addition, the magnitude decreases at a rate of approximately -20 dB per decade, and the phase decreases by -90 degrees, characteristics of a first-order system. Equivalently in the complex plane, as visual disturbance frequency increases, model response curves towards origin. Hence, a low-pass filter captures the main dynamics of the estimator model in both the time and frequency domain.

The estimator predicts the first-order, low-pass behavior of our previous shared integrator model [25]. However, unlike our previous paper, which explicitly proposed a low-pass filter, this type of filter emerged only from system dynamics and minimizing prediction error. Postural responses from our previous paper [25] also indicate tilt behavior can be captured with a low-pass filter. Hence, a low-pass filter is also used here to compare with experimental data. The model fit consists of a gain K, time constant τ, and include the possibility of a time delay t_{d}.

$$\frac{\theta}{\dot{\theta}_{\mathrm{VR}}} = \frac{K}{\tau s + 1} e^{-t_{\mathrm{d}} s} \tag{2.1}$$

Time delay t_{d} between the onset of visual perturbation and the start of the postural response accounts for possible latencies in visual processing and motor command signals to and from the brainstem [40].

2.3 Model Comparison with Experimental Data

2.3.1 Experimental Method

We tested the low-pass filter prediction by perturbing subjects visually in a virtual reality environment. We applied sinusoidal visual disturbances at a range of frequencies to identify the dynamic behavior of sensory integration. We also tested that the frequency response agrees with the time response from our previous paper [25]. Sixteen healthy adult subjects (12 female, 4 male, aged 22.8 +/-2.8 years) participated in this study and also in our previous study. All subjects had normal or corrected vision and reported no known injuries or disorders that might affect their ability to maintain balance. All subjects also

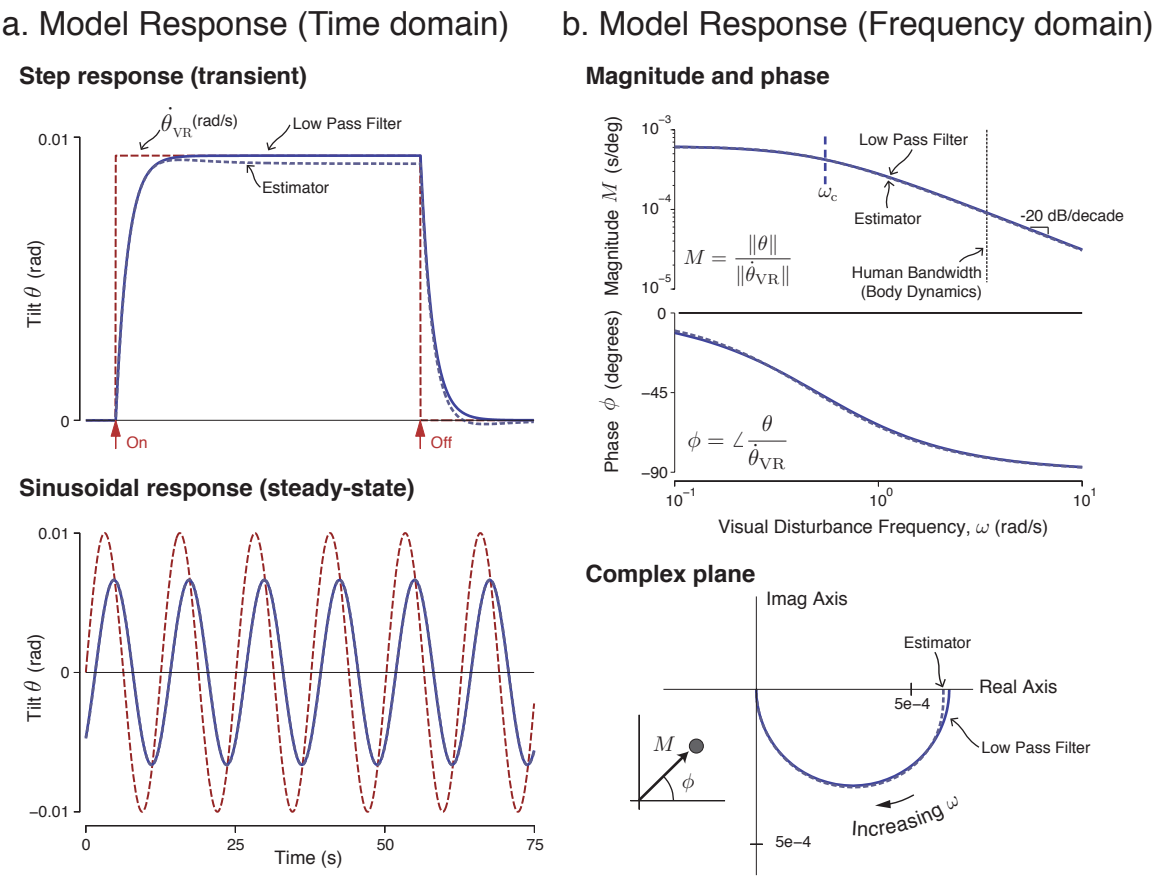

Figure 2.3: Comparison of estimator model (second-order) and low pass filter (first-order) in (a) the time domain and in (b) the frequency domain. Step response demonstrates transient responses while sinusoidal responses and frequency domain plots are concerned with steady-state behavior. The differences between two are minor in both domains. Hence, the low pass filter captures the dominant behavior of the estimator. Both models are shown without time delay, which would add a phase roll-off towards negative infinity.

provided informed consent according to institutional review board procedures.

Subjects were visually perturbed by an optokinetic field rotating about the head in the frontal plane (Figure 2.1). The visual field consisted of random white dots against a black background and rotated sinusoidally at a single frequency. We applied 11 frequencies, ranging from 0.1 rad/s to 5 rad/s, and the amplitudes were chosen to maintain a fixed maximum dot velocity of 15 deg/s across all frequencies. The trials were randomized and ranged from one minute to 6 minutes long, in which each perturbation had multiple cycles to obtain steady-state data. The visual field was also static before and after the perturbation. For the zero-stimulus standing trial, the visual field was static for 50 seconds. We recorded center of pressure (COP) response from force plates underneath the subjects' feet. The output postural response is body tilt θ, which we define as the center of pressure divided

by leg length, defined as the vertical height of pelvis markers above ground during quiet standing (0.958 ± 0.063 m, mean $\pm$ s.d.).

To compare each subject against the low-pass filter, we built a transfer function from frequency analysis of steady-state sinusoidal response. The transfer function was characterized by magnitude $M(\omega)$ and phase $\phi(\omega)$ data over a range of visual disturbance frequencies ω (Figure 2.4). Magnitude $M(\omega)$ describes the ratio of tilt response amplitude to visual disturbance amplitude, and the phase $\phi(\omega)$ shows how the subjects' response lagged behind the input signal. We used Fourier transform to determine if the tilt response was a sinusoidal dominated at the disturbance frequency, and if so, calculated its corresponding response amplitude and phase against the input stimulus.

We fit low-pass filter (Eqn 2.1) to each subject's frequency response (Figure 2.4). To determine gain K, time constant τ, and time delay t_{d}, a least squares algorithm, which minimizes the sum of residuals squared between data and model, was used . Magnitude and phase data were transformed into the real and imaginary data in the complex domain for the fit because ϕ will be the same value even if offset by a full rotation. We also fit to all subjects' data to a single low-pass filter and obtained a goodness of fit measure through the sum of the residuals squared. We qualitatively compared our frequency-based fit against step response fit from our previous paper [25]. We expect the two models to have comparable first-order, low-pass characteristics. For the comparison, the mean step response parameters were translated from the time domain into frequency domain, and the frequency-based fit results were transformed into the time domain using the following exponential equation:

$$y_{\text{s}} = A_{\text{s}}(1 - e^{-(t-t_{\text{ds}})/\tau_{\text{s}}}, \text{ for } t,\ t_{\text{ds}} \geq 0 \tag{2.2}$$

where y_{s} is the step response to a constant speed visual stimulus of 15 deg/s with response amplitude A_{s}, time constant τ_{s}, and time delay t_{ds}.

2.3.2 Results

We found that subjects responded to sinusoidal visual disturbances with sinusoidal postural tilt. The transfer function estimated from experimental data (N=16) appear to follow the estimator's low-pass filter trend (Figure 2.5). The response sinusoid was dominated by the stimulus frequency, and its magnitude decreased with increasing disturbance frequency. After the cut-off frequency, the magnitude of the slope descended at approximately 20 dB per decade. Phase also decreased and rolled-off towards infinity due to time delays.

Low-pass filter fit results yielded a time constant τ of 1.99 ± 1.11 (mean $\pm$s.d.) seconds.

a. Human Postural Response (Time domain)

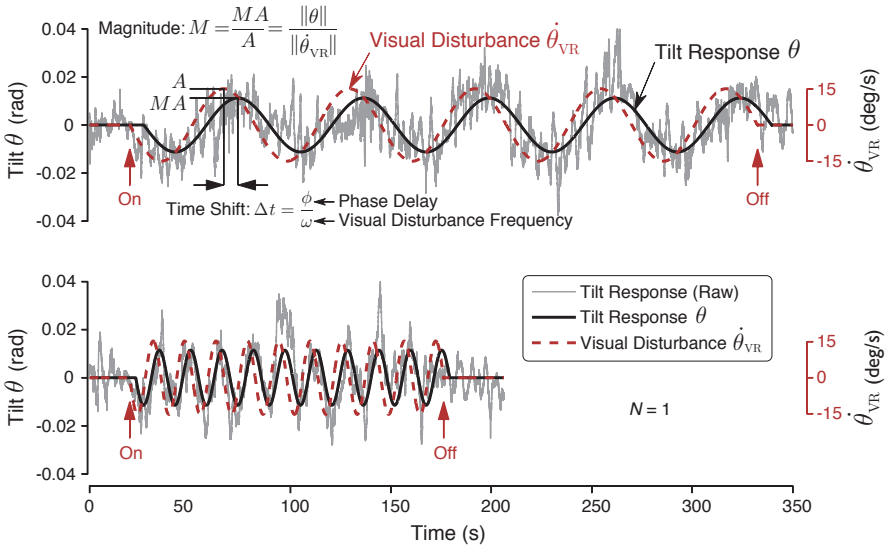

b. Human Postural Response (Frequency domain)

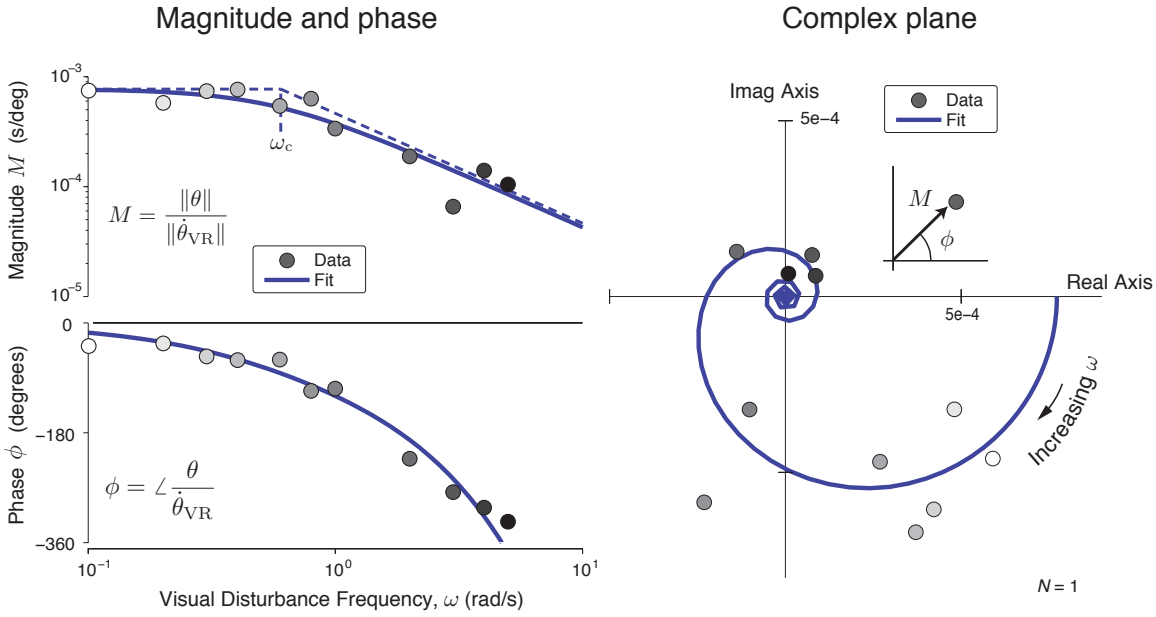

Figure 2.4: Representative tilt responses to sinusoidal visual disturbances from a representative subject. (a) Visual disturbances (dashed red) of two different frequencies, slow (top) and fast (bottom), yield raw tilt responses (solid gray) that may be approximated by sinusoids (solid black). (b) Tilt magnitude and phase data versus frequency (left) and in the complex plane (right) from the same representative subject (dots) and its first-order fit (solid line) in the frequency domain. The slope of the magnitude after the cut off frequency (vertical dashed blue) is approximately -20 dB/decade, a first-order behavior. Both magnitude and phase decrease as frequency increases with a phase roll-off towards negative infinity. Equivalently, in the complex plane, the data and model fit spiral towards the origin.

The gain K was 6.23e-4±3.28e-4 sec/deg, and the time delay t_d was 1.03±0.51 seconds. A fit to all subjects data gave similar results, with a time constant of 1.70±0.35 (mean ± C.I.) seconds, gain of 6.13e-4±6.00e-5 sec/deg, and time delay of 1.06±0.13 s. The sum of the residuals squared of the fit was 1.40e-5 (sec/deg)^2.

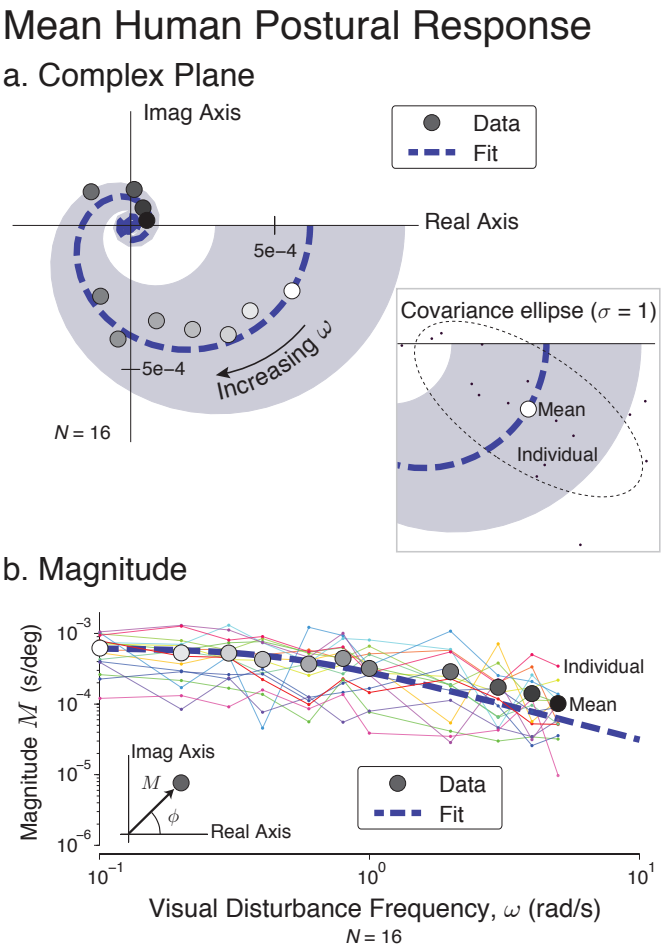

Figure 2.5: Tilt data and low-pass filter fits for all subjects in complex domain (N=16). (a) Mean tilt response across subjects (large dots) and mean (dashed blue line) and standard deviation (shaded) of subjects' fit parameters indicate that subjects' magnitude and phase decreased and spiraled towards origin with increasing frequency. Each subject's data is shown at the slowest input frequency (smaller dots) with a covariance ellipse (dashed black line). (b) Mean magnitude (large dots), subject magnitudes (small dots), and fit (dashed blue line) across subjects all decrease as s frequency increases.

With dynamical system, general characteristics predicted by the frequency response should be consistent with the time response. To assess time and frequency domain analysis of visual disturbance data, we qualitatively compared our low-pass filter fits with the step

response fits of trunk tilt from our accompanying paper [25] (Figure 2.6). Comparisons between responses demonstrate the first-order tilt response remains the same, but the time domain fit seems to have a greater time constant and time delay. The constant velocity stimulus may be more compelling because the optokinetic perturbation is sustained. This could also be due to differences in dynamics between trunk tilt and COP excursion.

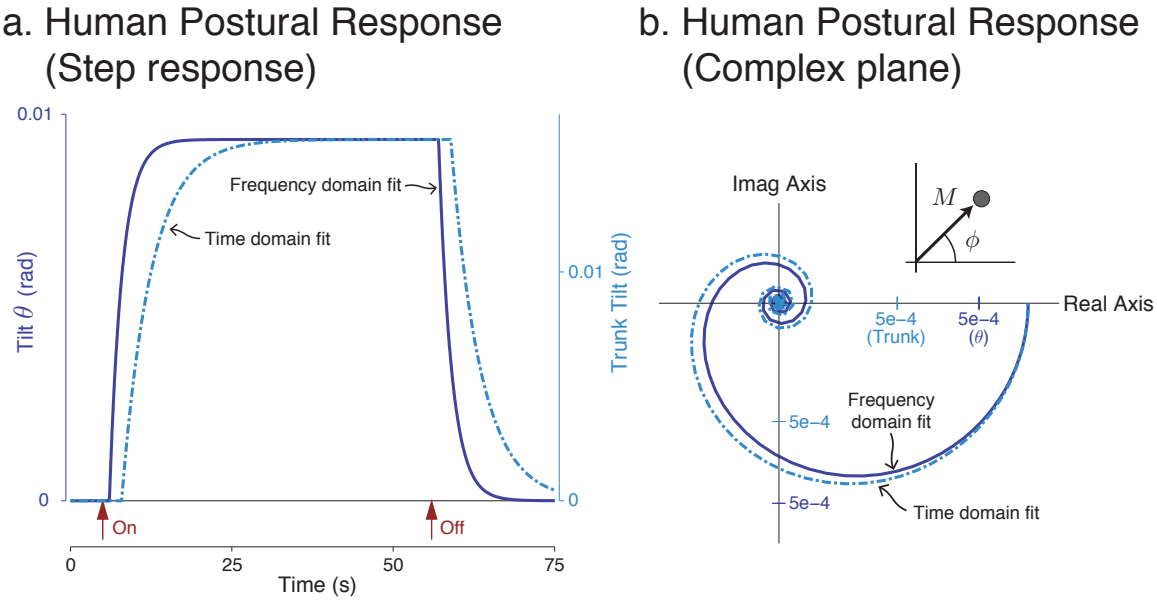

Figure 2.6: Comparison of fits in the frequency domain and time domain previously reported [25]) (a) as a step response and (b) in the complex plane. Step and frequency response of fit to frequency results (solid blue) and time domain fit of trunk tilt (dash-dotted blue, [25]) were similar, as both fits followed the same first-order, low-pass trend. Qualitatively, the time domain fits exhibited longer time constant and longer time delay.

2.3.3 Other Estimator Model Responses

We demonstrate the model's ability to reproduce postural responses to other perturbations and to sensors other than vision. These include a veridical shift in position and canal disturbances, such as from galvanic vestibular stimulation (Figure 2.7). A veridical shift in position may be modeled as a step in θ, which is equivalent to an impulse in angular velocity. The estimator demonstrates that this input affects all the sensors and predicts a quick shift in position in response. The model also predicts a response to a step in visual disturbance that is consistent with prior experiments [25, 36]. An exponential canal disturbance produces an exponential with a filtered peak, which qualitatively aligns with the experimental results of Haggerty et. al [25].

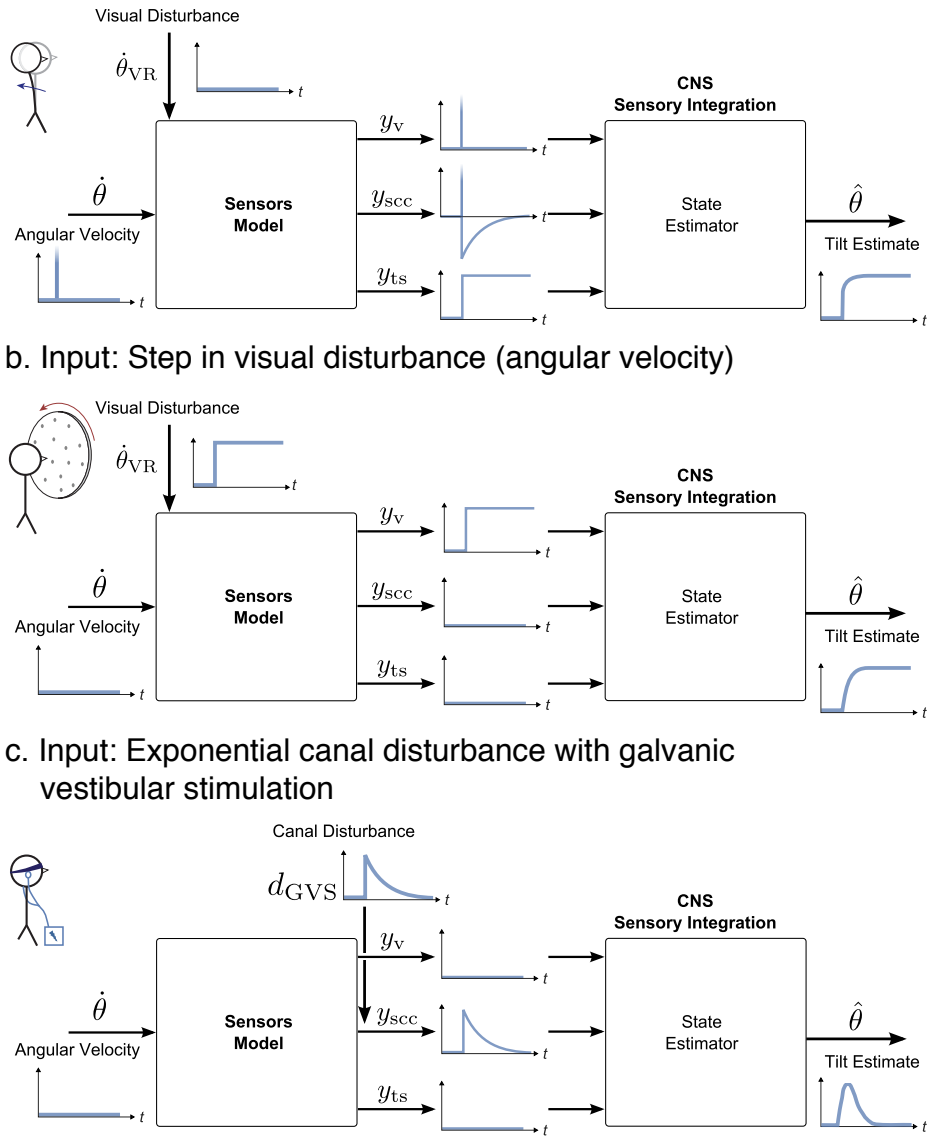

Figure 2.7: Estimator's tilt output $\hat{\theta}$ in response to other disturbances. (a) A voluntary step in position, equivalently an impulse in angular velocity, influences all sensors. The state estimator predicts a fast shift to the desired position. (b) Vision is perturbed with a constant angular velocity disturbance while the body is quietly standing. The estimator's response is a tilt in the same direction as the disturbance that eventually saturates. (c) To mimic effects of galvanic vestibular stimulation, the estimator is perturbed with a canal perturbation input (d_{GVS}) of a decaying exponential with a time constant T_{c}. The tilt estimate is a low-pass filtered exponential. Icons reproduced from [25].

2.4 Parameter Sensitivities

We varied sensor noise covariances to test that the estimator's first-order, low-pass behavior is robust against parameter changes. We also determined how transient and steady-state behaviors, such as the dominant time constant and gain, change with uncertainties in sensor information. Sensory weightings affect postural dynamics in relative terms. Specifically, it is the ratio of all three weightings, not the weighting value itself, which affects postural response. More reliable measurements have a smaller noise covariance weighting while a large weighting implies a noisier signal whose information is discounted, leading to diminished sensitivity. Heavy reliance on a signal may lead to hyperfunction while disregard of information may lead to hypofunction. To perform sensitivity analysis, we first determined the covariances for vision, canals, and tilt sensors from the low-pass filter fit. Then we modified these parameters from this nominal value.

Varying sensor parameters consistently resulted in models with low-pass filter behavior, albeit with different time constants and gains (Figure 2.8). If the canals information were more reliable than the visual or tilt sensor measurements, the time constant of the postural response would be greater than nominal. Even though vision is perturbed, the canals do not measure any tilt, and thus the body tilts slowly and with a much greater time constant. The magnitude of tilt is also less than nominal. If sensory measurements from vision had a smaller weighting, the body will tilt more because sensory integration relies highly on the erroneous visual information. However, the time constant remains the same and even increases slightly at small covariance weights. A possible explanation is these nominal sensory weightings were derived from perturbing vision, and there may be inherent distrust of visual information. Another is that canal dynamics have a greater effect on transient postural behavior than vision. However, despite changes in time constant and magnitudes due to sensor noise, the first-order, low-pass response still remains.

2.5 Discussion

The goal of this study was to test if an optimal state estimator could model sensory integration, specifically to explain postural responses to roll vection. We had previously proposed a shared integrator model, where the combination of vision, vestibular, and tilt sensor dynamics affect posture and was able to reproduce experimental behavior. We proposed an explanation for the neural integrator, based on minimizing prediction error. This optimization principle yielded a first-order, low-pass filter response, like the shared integrator, and experimental data in the frequency domain had similar dynamical behavior. Our

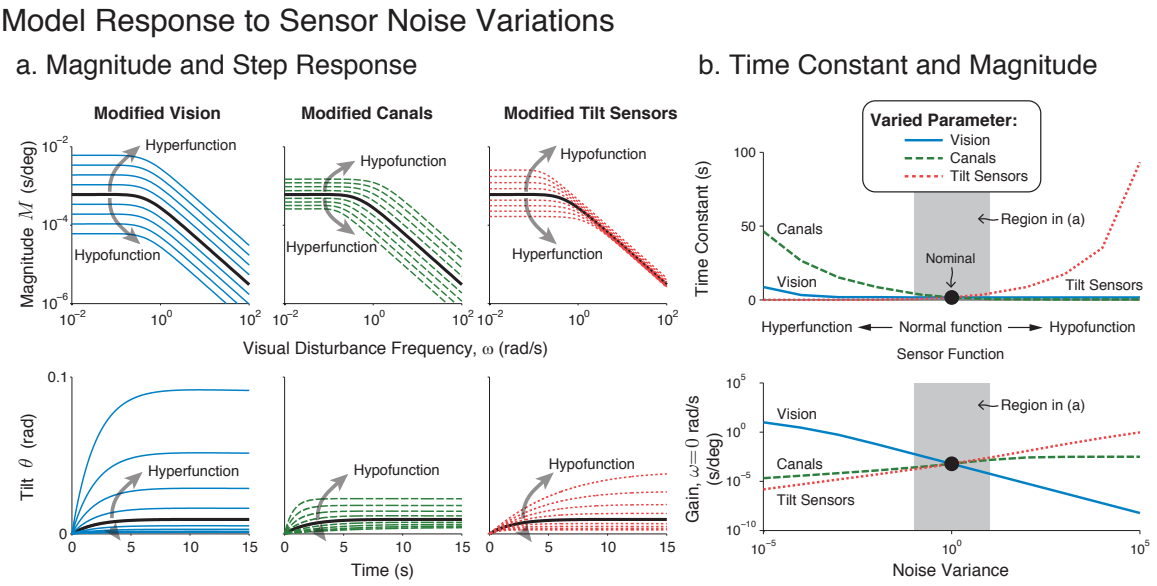

Figure 2.8: Effect of sensor parameters on (a) magnitude and step responses and (b) on the dominant time constant and gain. Sensor parameters were varied about experimentally-fitted nominal covariances. A smaller variance multiplier implies sensory hyperfunction while a large multiplier may lead to sensory hypofunction. Canal hyperfunction and tilt sensor hypofunction increases the time constant. However, time constant is relatively unchanged for changes in the vision parameter. Gain decreases with vision hypofunction but increases with hypofunction of the canals and tilt sensors.

parameter study also demonstrated that changes in sensor noise do not affect the overall behavior of the estimator. Time constants and magnitudes may be affected by weightings, but the first-order, low-pass filter behavior is consistent. The frequency-domain fits were also able to reproduce qualitatively similar responses to previous time domain fits [25]. Hence, the estimator can predict human tilt behavior under different types of visual perturbations. The estimator model can also reproduce postural responses from disturbances to canals as well as from a veridical position shift. Hence, the estimator could be a sufficient simple model for sensory integration.

While the interaction of multiple sensor dynamics has already been demonstrated in other posture models [9, 24, 37], this estimator is relatively simple, and therefore conceptually similar to visual-vestibular models [12, 57, 58]. In particular, the estimator, which includes tilt sensors, still produces behavior that is consistent with a shared integrator, like the neural integrator model [25]. Hence, the slow dynamics of the canals affect postural response, even if they are not directly stimulated. The response seems to compensate for canal dynamics, similar to how vision compensates for the high-pass filter dynamics of the canals in head movements [58].

To combine multiple sensory information, state estimators rely on an internal model to enable sensory predictions and an error signal between measured sensory outputs and predicted sensory feedback, components of which could be biologically occur in the cerebellum [40, 52]. The cerebellum receives multiple sensory data and efference copies, and evidence suggests that the cerebellum plays a key role in error correction [41]. The cerebellum has also been shown to use internal models for limb movement anticipation to control torque interactions among multiple limbs. Adaptation may also occur within the cerebellum to maintain accurate internal models. The low firing frequencies of climbing fibers, for example, are too slow for real-time error corrections. However, they can modulate the response of neurons to mossy fiber inputs and thus may be involved in error detection to enable future corrections.

There were several limitations in this study. We did not consider controller dynamics and used estimated tilt as actual tilt. The feedback loop seems relatively fast, as indicated by the comparison between measured body bandwidth and cupula and low-pass filter time constants. We used center of pressure as a measure of body tilt and did not consider multi-segment behavior. Qualitative differences in time constant between trunk tilt (previously reported [25]) and center of pressure could be due to differences in tilt measures. The sinusoidal perturbations were single frequency sinusoids and are therefore potentially predictable to the subject. Our linear model was also unable to capture nonlinear behaviors, such stimulus-dependent onset time delays [9] and changes in postural behavior with and without vection [65]. We also fit tilt response with a constant set of sensory weightings. However, Peterka [54] showed that as visual stimulus increases, vestibular information is utilized more as vision information is discounted. Hence we were unable to capture changes in sensory weightings, if any, during the experiment. However, based on the parameter studies, we expect an estimator model with changing, or adaptive, noise parameters would still demonstrate dominant behavior consistent with a low-pass filter.

2.6 Appendix. Details of sensors and estimator model

We model sensors with simple, first-order dynamics (previously reported [25]). The input to the sensors is angular velocity, and vision measures angular velocity input, the canals are a high place filter, and the tilt sensors are an integrator. Define the sensors states as $x_1 = \theta_{\text{scc}}$ and $x_2 = \theta$, as the angular velocity input, and vision, canal, and tilt sensor measurements as outputs. In state-space form, the sensor transfer functions are $\dot{x} = Ax + Bu + Bw$, $y = Cx + Du + Dw + v$, where

$A = \begin{bmatrix} -\frac{1}{T_c} & 0 \\ 0 & 0 \end{bmatrix}$, $B = \begin{bmatrix} 1 \\ 1 \end{bmatrix}$, $C = \begin{bmatrix} 0 & 0 \\ -\frac{1}{T_c} & 0 \\ 0 & 1 \end{bmatrix}$, and $D = \begin{bmatrix} 1 \\ 1 \\ 0 \end{bmatrix}$. Noise signals w and v are zero-mean, Gaussian white noise. Process noise w models uncertainty in disturbances and in the accuracy of the sensors internal model, and measurement noise v models uncertainty in sensor reliability.

State estimators fuse multiple sensor information to produce a tilt estimate using internal models and a particular set of process noise and sensor noise. Estimators are optimal when minimizing the mean-squared error between measurements and outputs predicted by its internal model. We design an estimator with an internal model of the body and sensor dynamics by using the same state-space matrices. The estimator in state-space form is:

$$\begin{aligned} \dot{\hat{x}} &= A\hat{x} + Bu + L(y - \hat{y}) \\ \hat{y} &= C\hat{x} + Du \end{aligned}$$

In state estimation, design of gain L dictates estimator dynamics. Specifically, L determines how the estimated states converge to the actual states. With optimal estimators, the gain depends on minimizing the mean-squared estimation error $y - \hat{y}$ subject to the W, process noise covariance, and V, measurement noise covariance.

We treat the measurement noise of the sensors to be independent and uncorrelated,

$$V = \begin{bmatrix} V_{\text{vision}} & 0 & 0 \\ 0 & V_{\text{canals}} & 0 \\ 0 & 0 & V_{\text{tilt sensors}} \end{bmatrix} \tag{2.3}$$

where each entry in the diagonal matrix is a scalar. The process noise is scalar W. To derive the solution, we solve for P in the Riccati equation to find L [11].

$$PA^T + AP - (PC^T + S)R^{-1}(CP + S^T) + Q = 0 \tag{2.4}$$

where $R = V + DWD^T$, $Q = BWB^T$, and $S = BWD^T$. The solution to the Riccati equation yields optimal estimator gain:

$$L = (PC^T + S)R^{-1} \tag{2.5}$$

where $L = \begin{bmatrix} L_{\text{v}} & L_{\text{scc}} & L_{\text{ts}} \end{bmatrix}$. The first column of L pertains to optokinetic stimulus while the second column relates to canal inputs. Hence, the estimator models from visual perturbation to estimated tilt and from galvanic vestibular stimulation to estimated tilt are subsets of the above model.

CHAPTER 3

Multi-limb coordination model of lateral stabilization for one-legged balance

3.1 Introduction

Balance on one-leg is a challenging but important task. Each step during walking, for example, involves a brief period of one-legged balance and control until the next foot fall. One-legged balance is more difficult than two-legged balance because base of support, a key contributor towards balance control [28], is reduced. Therefore one-legged balance is also frequently used as a clinical test to assess fall risk, as ability [18,69], duration [6,8,66], or postural steadiness [23, 32] could be a predictor of falls. However, these measurements do not explain or assess balance strategies, which are more often investigated for two-legged balance. Hence it is unclear if current postural control models, such as inverted pendulum models (e.g. [20, 28, 71]) and feedback control models (e.g. [39, 54]), can be applied to one-legged balance. Except for a few cases (e.g. [27, 48]), balance strategies for one-legged balance have not been investigated.

The human body is inherently unstable due to inverted pendulum dynamics and thus requires stabilization. The goal of balance control, modulated by the central nervous system (CNS), is to maintain the body center of mass (COM) over its base of support (BOS), nominally the feet [28]. Multiple processes are necessary for stability, such as appropriate movement strategies, sense of orientation, control of body dynamics, and biomechanical constraints such as base of support, quality of standing surface, and body configuration [28]. Failure in any one of these, due to aging for example, may lead to loss of balance. Balance adjustments may occur through a series of feedback loops that may be fast spinal reflexes or involve processing of multiple sensory data [40, 54]. These feedback loops may be modeled as a feedback control law (e.g. [39]), where weighted sums of gains determine the relationship between body states and torques. Feedback gains have been previously

used, for example, to investigate the relationship between ankle and hip torques and angles as a function of perturbation magnitude [51] and to investigate balance under sensory organization test (SOT) conditions [40].

Humans stabilize their balance through a variety of actions, including adjustment of center of pressure and movement of the limbs. Most balance control studies investigate the two-legged balance in the sagittal plane, and these strategies are known as the ankle strategy and the hip strategy [29]. The ankle strategy, or center of pressure strategy, is used when standing on firm surfaces or to respond to small disturbances. The hip strategy is used for large balance corrections or when standing on compliant surfaces. Use of ankle and hip strategies also scales with perturbation size, as demonstrated by backward platform perturbation experiments [51]. Similarly, the strategies for one-legged lateral balance include use of center of pressure and use of limb movement to create angular momentum [27]. Center of pressure is nominally used during normal one-legged balance, but angular momentum seems to contribute more towards balance when standing on a narrow ridge [27, 48]. In particular, angular momentum is used to modulate the lateral ground reaction force, which moves the body center of mass indirectly.

The difference between sagittal plane and lateral plane balance is that one-legged balance involves multiple limbs. Few studies have considered how multiple limbs should be coordinated and in what ways to keep the body stabilized. It is also unclear which limb may contribute most towards balance. The nominal coordination strategy may also become infeasible due to environmental conditions, such as reduced base of support (BOS), and thus require adjustments. We hypothesize that one-legged balance is similar to two-legged sagittal plane balance and propose a simple balance model based on angular momentum principles to show that limbs should be accelerated in the same direction as the displaced stance leg for stability. Since inertia is important in imparting torques, we hypothesize that limb contribution will correlate with mass. We expect the trunk to contribute the most and arms the least. Similar to the platform perturbation experiments, we expect that humans compensate for BOS constraints by adjusting feedback gains between body segments.

3.2 Methods

To examine coordination strategies for one-legged balance under a variety of environmental conditions, we developed a simple model of one-legged balance control based on dynamic principles and compared model expectations to experimental results from subjects performing balance under normal environmental conditions and with base of support constraints. One-legged balance is modeled as a simple multi-link model with a main

pelvis mass atop an inverted pendulum stance leg, and several generic appendages that may be moved to control balance. We compared the feedback control law for stabilizing this model against empirical control gains derived from subjects during several one-legged balance conditions.

3.2.1 Multi-Pendulum Model of Balance

We use a simple inverted pendulum model to illustrate how angular momentum may be used for balance. The model is a massless inverted pendulum stance leg with a main mass at the top (Figure 3.1). The stance leg has mass M and length L and is pinned to the ground. The stance leg's ankle torque can be used to control the main mass, but the ankle can only exert limited torques against the ground. Hence, the stabilization of the stance leg about the vertical requires that torques be exerted against the inertia of the trunk, arms, and opposite leg. In the case of our simple model, we generalize this into a momentum wheel with inertia mr^2 to impart a torque. To produce an appropriate restoring torque, impulse-momentum principles dictate that the net torque acting on the momentum wheel should be in the same direction as the angular displacement of the stance leg. With no stance ankle torque, the only stabilization possible is from the momentum wheel. In our example, the stance leg is displaced to the left, and therefore the momentum wheel should be rotated counter-clockwise. That imparts a reaction torque on the stance leg, which pivots about the foot. The pivot constraint induces a ground reaction force directed to the right, which therefore causes the body COM to be restored in that direction as well.

Angular momentum strategy may be used regardless of actuation at the stance ankle. In contrast, using a linear momentum strategy is not feasible if no ankle torque exists. The linear momentum strategy uses a mass m on a massless horizontal linear slider to move the main mass. The mass should be slid to the left if the stance leg is displaced to the left. The force F in displacing the slider ball to the left will impart a reaction force on the main mass to the right. However, the force F from the sliding mass has no effect on the lateral acceleration of the center of mass:

$$\text{COM}_{\text{LM}} = -\frac{gL(m+M)q - gmx}{L(m+M)} \tag{3.1}$$

where q is the stance leg angle, x is the slider mass displacement, and g is gravitational acceleration. In contrast, the torque $-T$ by the momentum wheel onto the stance leg does affect the lateral COM acceleration:

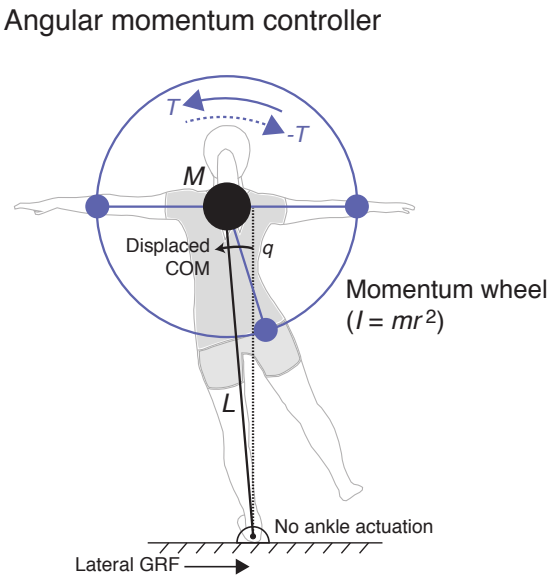

Figure 3.1: Model of angular momentum for lateral balance control. The human is generalized as an inverted pendulum stance leg with a main mass on top and a momentum wheel for control. The momentum wheel is accelerated in the same angular direction as the displaced COM, which produces an equal and opposite torque $-T$ onto the stance leg. Because the stance leg is pinned to the ground, the torque causes a lateral ground reaction force, which moves the COM indirectly over the ground contact point, which is in the stabilizing direction.

$$\text{COM}_{\text{MW}} = -\frac{-T + gLM \sin q}{L(m + M)} \tag{3.2}$$

Hence, stabilization is not feasible with the slider mass unless the sliding mass can be detached from the body.

The simple momentum wheel model can be generalized into multiple pendulums that may move independently for balance. Hence, we hypothesize that the net torque exerted on the trunk, swing leg, and arms should all be directed in the same direction as any displacement of the stance leg. Defining feedback gain as torque on segment divided by stance leg displacement, the hypothesis is equivalent to stating that the net gain should be positive for stability. Since inertia is important in moving the COM, we expect the trunk to contribute the most and the arms the least towards balance. In addition, sagittal plane research has indicated that feedback gains may scale with perturbation size [51]. Hence, a second prediction is that reduced base of support will lead to increased limb gains to compensate for reduced center of pressure.

3.2.2 Experiment

To test the hypothesis that the limbs should be rotated in the same angular direction as the displaced stance leg, we measured one-legged balance behavior from nine healthy adult subjects using spontaneous noisy fluctuations as the perturbation. All subjects (8 female, 1 male, aged 23±3 years, mean ± S.D.) had reported no known injuries or disorders that might affect their ability to maintain balance. All subjects also provided informed consent.

Subjects balanced on their stance leg while their swing leg, trunk, and arms may be used to control balance. We compare all conditions against a baseline trial "Normal" (Figure 3.2). In this condition, subjects balanced on one leg with eyes open and used all available limbs if needed. The size of their lateral base of support was their foot width. The starting arm position was perpendicular to the trunk, and the arms were allowed to move about this nominal position.

We also applied three widths for base of support. Reducing the base of support indirectly reduced the effectiveness of using ankle torque to balance. In "Wide," subjects' standing foot was strapped to a block that provided a wider-than-normal base of support (0.127 m, 5 in). In "Narrower," subjects stood on a 0.0508 m (2 in) wide block, and in "Narrowest," subjects stood on a 0.0254 m (1 in) wide block. Average foot width at the widest point was 0.1000±0.0065 m. Block lengths were longer than the subjects' foot.

Subjects balanced on their non-kicking leg, which was the left foot for all subjects. The trials were randomized and ranged from 12 seconds to a maximum of 60 seconds, depending on the subjects' ability. One subject did not have a Narrow or Narrowest trial due to equipment failure. Motion capture recorded joint angles and angular velocities, and joint torques were calculated from inverse dynamics. The measurements were band-pass filtered to remove slow limb drifts and noise. Center of pressure (COP) and center of mass (COM) excursions were also recorded.

Subject joint kinematics and kinetics measurements are defined as follows. Stance leg angle is the angle between the stance leg's shank and the ground. Trunk angle is between torso and the stance thigh. Swing leg angle is between swing leg thigh and pelvis. Right arm angle is measured between right upper arm and torso, and left arm angle is measured between left upper arm and torso. The same relationships hold for the angular velocities. Trunk torque is defined as the stance hip moment, swing leg torque is swing hip torque, and right arm torque is right shoulder torque. Stance foot torque is the product of COP and vertical ground reaction force, and stance ankle torque was also measured.

We empirically derived feedback gains using a least-squares regression. The feedback gains K of a simple control law (Eqn 3.3) describe the relationship between torques applied to limbs T and the joint angles q and angular velocities $\dot{q}$.

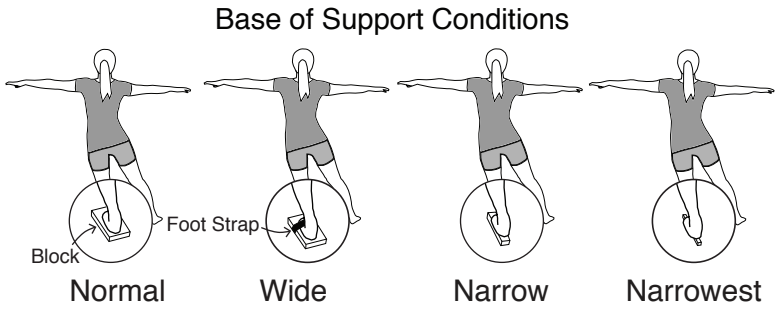

Figure 3.2: Baseline one-legged balance condition (Normal) and various base of support conditions. The base of support for Normal is the stance foot width. Base of support for Wide condition is wider than foot width, and the Narrow and Narrowest conditions are narrower than foot width.

$$u = Kx \tag{3.3}$$

where:

$$u = \begin{bmatrix} T_{\text{trunk}} \\ T_{\text{swing leg}} \\ T_{\text{stance foot}} \\ T_{\text{arms}} \end{bmatrix}_{4\times1} = \begin{bmatrix} k_{\text{Ttrunk}} & \cdot & \cdot & \cdot & \cdot & \cdot & \cdot & \cdot \\ k_{\text{Tswing leg}} & \cdot & \cdot & \cdot & \cdot & \cdot & \cdot & \cdot \\ k_{\text{Tstance foot}} & \cdot & \cdot & \cdot & \cdot & \cdot & \cdot & \cdot \\ k_{\text{Tarms}} & \cdot & \cdot & \cdot & \cdot & \cdot & \cdot & \cdot \end{bmatrix}_{4\times8} \cdot \begin{bmatrix} q_{\text{stance leg}} \\ \dot{q}_{\text{stance leg}} \\ q_{\text{trunk}} \\ \dot{q}_{\text{trunk}} \\ q_{\text{swing leg}} \\ \dot{q}_{\text{swing leg}} \\ q_{\text{arms}} \\ \dot{q}_{\text{arms}} \end{bmatrix}_{8\times1} \tag{3.4}$$

We only define the relevant gains of interest, which are in the first column of K. These gains are related to the stance leg angle, our proxy for the COM, and the sign of these gains indicate how limb torques should be applied depending on the angular displacement of the stance leg. Applying our hypothesis to the control law results in a positive net gain for the first column of the gain matrix. Equivalently, the limb torques should be positively correlated with stance leg angle (Figure 3.3).

We fit one gain matrix for each trial using a least-squares algorithm. To normalize across subjects of differing weights and heights, angular velocities and torques were normalized to gravitational acceleration g, subject mass M (58.6$\pm$6.25 kg), and subject leg length L (0.851$\pm$0.048 m) prior to regression to yield dimensionless quantities. The sign of the net gain is $\text{sgn}(k_{\text{Ttrunk}} + k_{\text{Tswing leg}} + k_{\text{Tstance foot}} + k_{\text{Tarms}})$, comprising the limbs that

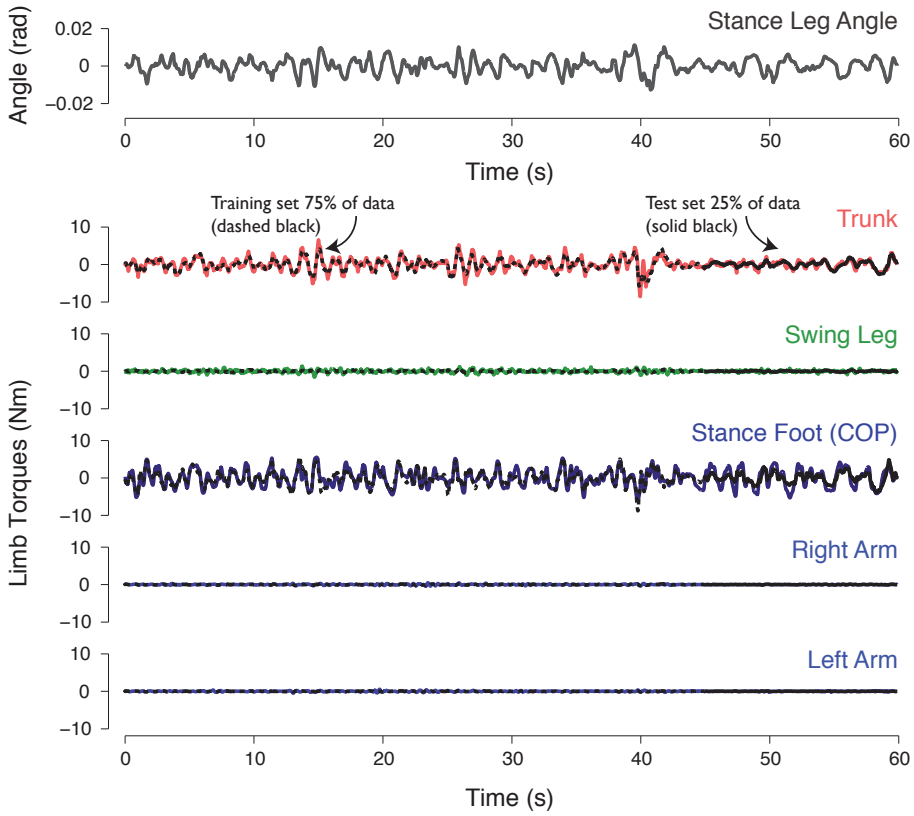

Figure 3.3: Sample stance leg angle and limb torques from one subject. The correlation between the torques and angle determine the sign of the gains in the gain matrix and how the torques are applied due to the displaced stance leg. Trunk and stance foot seem to impart greater torque on the stance leg than the swing leg and arm. Overfitting was checked by determining how well the training model (dashed black), derived from the first 75% of data, predicted the last 25% of the data (solid black).

affect the stance leg. Arms were included in the sum even though they act on the stance leg indirectly. Trunk has the highest inertia among swing leg and arms, and therefore is expected to exert the largest torque and have the largest gain of the limbs. Stance foot is also expected to impart large torques and result in a large gain because it acts against ground. We also checked for overfitting by fitting to the first 75% of the data and comparing the predictions of the training model to the last 25% of the data. In addition to feedback gains, we also investigated limb movement variability through root mean square of limb angles and COP and COM variability.

3.3 Results

Subjects' controller gains for all BOS conditions were net positive. This is consistent with our prediction that limbs should be accelerated in the same angular direction as the stance leg to stabilize. Net gain also scaled with base of support. Subjects modified individual limb gains, limb movement variability, and COM and COP variability to compensate.

The net gain increased with reduced BOS condition but remained positive (Figure 3.4). Net gain at Narrowest was significantly different from Normal ($p = 0.0087$), and the net gain at Narrow was significantly different from Narrowest ($p = 0.0257$). Nominally, under Normal balance, stance foot (COP) produced the dominant gain. However, reducing BOS decreased COP excursions, which contributed to a less effective stance foot for balance. Both Narrow ($p = 0.0019$) and Narrowest ($p = 0.0012$) conditions were significantly different from Normal.

Larger gains from available limbs were utilized to compensate for decreased gain in stance foot. Compared against Normal, the trunk and swing leg gains were significantly different at Narrow ($p = 0.0133$, $p = 0.0299$) and Narrowest ($p = 0.0013$, $p = 0.0064$). The arms were also significantly different at the Narrowest condition ($p = 0.0193$). The trunk, in particular, contributed 66% of the net gain at the narrowest BOS condition compared with 6.3% at the normal BOS condition. The other body segments may help balance, but their relatively low mass seems to correlate with the small size of their gains. Coordination strategy for Wide condition was not different from Normal balance. Hence, subjects did not seem to take advantage of the wider base of support to reduce limb gains.

We fit one time-invariant gain matrix for each subject's trial. The regression produced reasonable fits ($R^2 = 0.727 \pm 0.109$), and the model did not seem to be overfitting. Fits of the training model to the test data yielded R^2 of 0.639 ± 0.173.

Limb movement variability also increased with reduced BOS. (Figure 3.5). Arms seemed to produce the most movement during Normal, followed by trunk, swing leg, and stance leg. All limbs' movement increased with narrower base of support. Stance leg variability was significantly different at Narrow ($p = 9.55e - 4$) and Narrowest ($p = 2.2526e-5$). Trunk variability was significant at Narrowest ($p = 3.69e-4$) and Narrowest ($p = 4.75e - 4$), as was for the swing leg (Narrow $p = 0.0225$, Narrowest $p = 2.204e - 4$). Arm variability was significant for Narrowest only ($p = 0.011$). Qualitatively, stance leg variability increased at a shallower rate, and the arms increased at the steepest rate. This might be because the stance leg, as the limb closest to the ground, may have a greater effect on the body with small movements.

BOS reductions also affected COP and COM excursions (Figure 3.6). As expected,

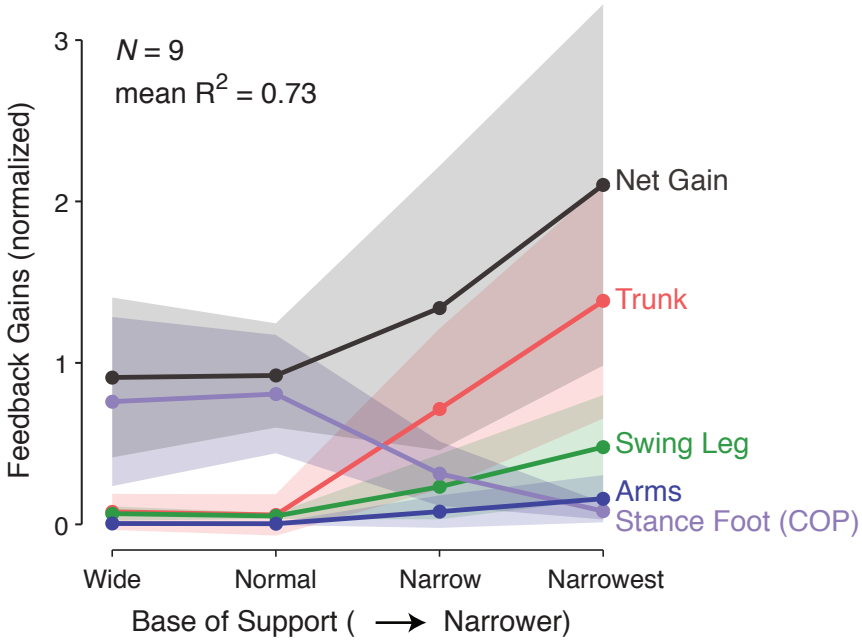

Figure 3.4: Empirical feedback gains of subjects ($N = 9$) balancing on one-leg under varying base of support widths ($R^2 = 0.727 \pm 0.109$). Net gain was positive under all conditions. Under Wide and Normal condition, stance foot (COP) dominated. As BOS decreased, the trunk, swing leg, and arms gains grew to compensate.

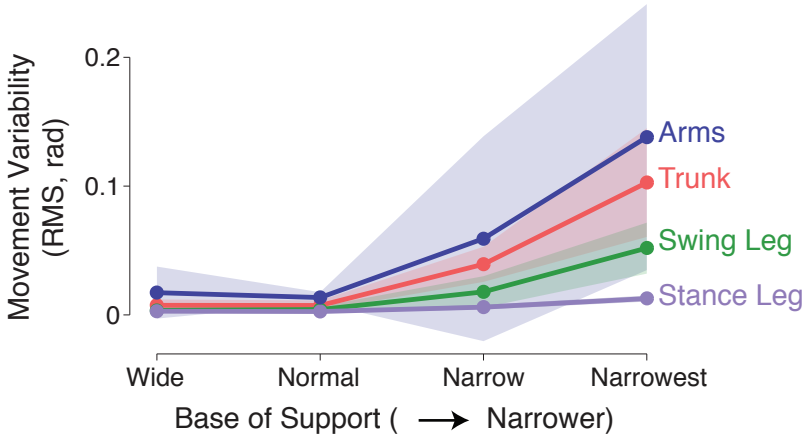

Figure 3.5: Movement variability of all the limbs, measured by RMS, increased as base of support widths decreased. In general, the arms have the greatest variability while the stance foot has the least.

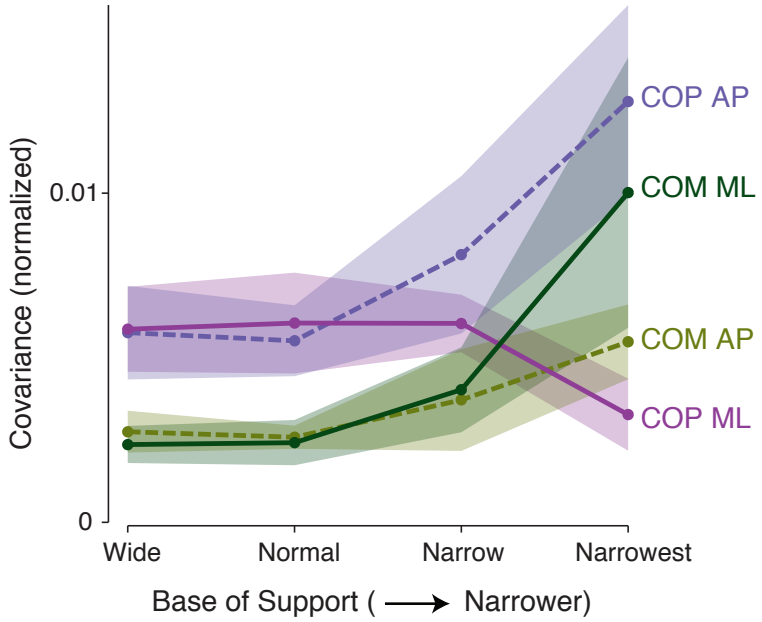

Figure 3.6: Covariance of COM and COP excursions in the anteroposterior (AP) and mediolateral (ML) directions as base of support varies. BOS reduction lead to decreased ML COP variability and increased ML COM variability. COM and COP in the AP direction also increased with reduced BOS.

reduced BOS lead to a decreased COP variability (Narrowest $p = 0.0025$) in the mediolateral (ML) direction. ML COM covariance also increased (Narrow $p = 0.0119$, Narrowest ($p = 0.0016$), perhaps due to increased movement from free limbs and the lack of control authority with the stance ankle. The reductions in BOS should only affect the frontal plane, since the changes were only in width, as the length of the blocks were constant. However, sagittal plane changes were observed. Both COP (Narrow $p = 0.0108$, Narrowest $p = 8.890e - 5$) and COM (Narrowest $p = 1.5968e - 4$) in the AP direction increased, despite no change in the available length-wise area that could be used for balance. It is unclear if the changes in AP direction were intentional to compensate for BOS or the unintentional result of a more unstable system.

3.4 Discussion

Multiple limbs contribute towards one-legged balance by rotationally accelerating in the same angular direction as the displaced stance leg. To accommodate BOS constraints, humans amplify the overall gain and redistribute feedback gains among the unconstrained limbs. Other than the stance foot, the trunk appears to have the largest contribution towards the restoration torque on the stance leg with a gain modulated based on the base of support.

Inertia of the controlling limb seems to be correlated to the size of its effect on the stance leg angle. Limb movement variability also increased to compensate for decreased BOS, with arm angles exhibiting the greatest variability. In the ML plane, BOS reductions led to decreased COP and increased COM excursions. However, sagittal plane COM and COP were also affected by the BOS constraints.

The main one-legged balance strategy is analogous to the ankle and hip strategies of two-legged sagittal plane balance (e.g. [29]). In both cases, ankle strategy, or COP, serves as the main balance mechanism until large perturbations or base of support conditions require the use of angular momentum, as also suggested by Hof [27]. Multiple limbs are involved in lateral balance, and we take this concept a step further by determining individual limb contributions, similar to Otten [48], but in terms of feedback gains. The gains for one-legged balance also scaled gradually, similar to gains found in other studies [51]. Hence, the CNS does not seem to use different strategies for one-leg versus two and may also use the same balance control for both planes.

We interpreted one-legged balance strategies in terms of feedback control. However, feedforward control is possible, where responses are preprogrammed and do not require sensory feedback. It is possible that the gains operate in an open-loop and are part of a library of preprogrammed responses in the CNS. Since it is difficult to differentiate between the two without further study, the actual contributions of feedback and feedforward control towards balance responses is unknown.

Here we only considered the gains related to the stability of the stance leg angle. However, there are other elements in the gain matrix that may contribute towards balance. In particular, the gains related to stance leg velocity should also be positive for damping. We found that the net velocity gain was negative, meaning a negative correlation between limb torques and stance leg velocity. However, these velocity gains are small compared to the gains on stance leg angle. Therefore, the magnitude of the angle gains seem to contribute more than the angular velocity gains towards a stabilizing torque. Other elements in the gain matrix are also small relative to our gains of interest.

We only considered frontal plane motion in our gain analysis, decoupling balance in the sagittal plane from the frontal plane. However, the COP and COM results show that sagittal plane motion is affected by reduced BOS. Perhaps this is because it is difficult to move in only one plane. Limb corrections might have out-of-plane components, and the greater variability in movement might further destabilize the subject, increasing the AP COM excursion and requiring more COP to compensate. Alternatively, there may be cross-terms between balance strategies of these two planes, perhaps including the transverse plane, and thus lateral BOS reductions would require compensation from all components

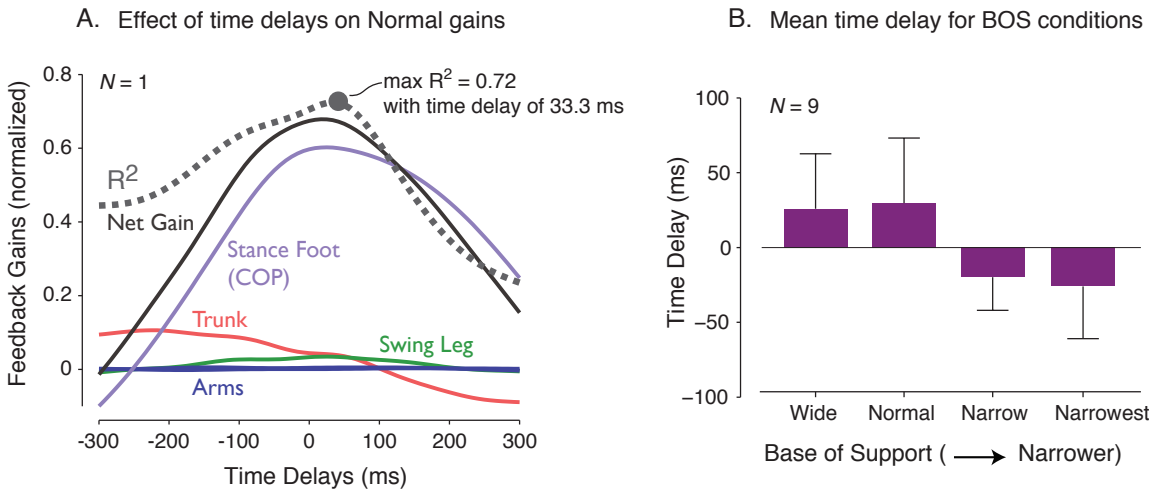

Figure 3.7: Effect of time delays on regression results across base of support conditions. (A) The effect of time delays on feedback gains and goodness of fit (N=1). In this example, the maximum R^2 occurred at a time delay of 33 ms. (B) Mean time delay (N=9) show a non-significant decreasing time delay as BOS decreases. Time delay was chosen based on maximum goodness of fit.

of movement.

Stance foot gain, which includes COP, and lateral COP covariance decrease in different ways with reduced BOS. Stance foot gain decreased from Normal to Narrowest, but COP variability only decreased at Narrowest. The effective width used for COP during Normal could be similar to Narrow, while the relationship between COP and stance leg angle may change more drastically. Hence balance strategies that occurred during Narrow were not necessarily captured with force plate measurements.

We did not include time delays in our model. Time delays between limb torques and changes in limb state are possible from latencies in sensing and in motor command signals for CNS feedback control. Latencies in human feedback loops range from 30 ms to more than 90 ms ([40]). Anticipatory movements are also possible, as the body may act without waiting for sensor feedback [29]. Therefore, we explored time delays between -300 to 300 ms and calculated the gain matrix and R^2 value as time delay varied (Figure 3.7). We then compared the time delay that corresponded to the best R^2 value. Time delays decreased as BOS became narrower but not significantly. R^2 with 0 time delay was 0.727 ± 0.109 and with the "best" time delay was 0.7491 ± 0.103. Hence, including time delays did not greatly improve the fit between limb states and torques and had little effect on our results. Since each limb may have its own individual time delay, it is not surprising that one general time delay did not change the results.

We treated the body as a simple multi-pendulum system in the gain regression, with

trunk, arms, and legs as pendulums. However, there may be multiple modes to each limb. For example, the trunk can bend at each vertebra, and the arms can bend at the elbow. We also did not study how the pelvis contributes towards balance. However, since the bulk movement of each limb contributed in a dynamically sensible manner, the net effect of the joint within our limbs of interest should still contribute positively towards stabilizing the body center of mass.

We also fit linear, time-invariant feedback gains to experimental data. This does not capture gain changes, if any, that occur during each trial, or effects of nonlinear gains. We also did not consider slow movement drift and removed them with a high pass filter prior to analysis. However, this simple model fit could reproduce experimental data reasonably well ($R^2 = 0.727 \pm 0.109$). Hence the body controller may be more concerned about body dynamics about some nominal position, such as upright stance, and uses some form of linearization for control. The feedback gains also scaled with reduced BOS, which is a nonlinear phenomenon. Balance control may be similar to gain scheduling, where linear gains are used, but gain values may change depending on environmental conditions.

One-legged balance is used clinically to assess fall risk, but the tests do not typically quantify the patient's balance strategies. The criteria to achieve a "good" balance score also varies by test [6, 8, 66]. Our model of lateral balance may provide a more mechanistic balance assessment tool. Specifically, the model can indicate if the balance strategy is dynamically sensible and how each limb contributes towards balance. Comparison of gains from older adults and its potential use for fall risk assessment is one future study.

CHAPTER 4

Momentum usage in a simple model of sit-to-stand movement

Many human motions are performed with energetic economy, which depend on mechanical work and other aspects of muscular effort. For example, preferred step frequency and preferred step width during walking coincides with minimum energetic cost [16, 45]. For a sit-to-stand (STS) movement, also known as chair rise, the theoretical minimum required for mechanical work is the gravitational potential energy gained between the two positions. An economic motion might approach this minimum if negative work could be avoided.

Two main strategies of chair rise differ by the use of momentum [56]. In the dynamic method, the trunk generates forward momentum prior to seat-off and transfers the forward momentum into vertical momentum at seat-off. The second method involves repositioning the center of mass and the feet prior to seat-off so that they are aligned vertically. Then the joints are slowly extended, nearly quasi-statically. There is significant forward velocity at seat-off in the first method, and little in the second method. Both strategies eventually place the center of mass (COM) directly above the base of support (BOS), but momentum allows that to take place after the chair has been unweighted. The second method seems "safer" than the first, more dynamic method, because the COM is always above the base of support during the rise phase.

Older adults, for example, especially those with functional impairments, favor a strategy that repositions their COM closer to their base of support prior to seat-off [30, 31, 59, 61]. This avoids momentum usage and thereby employs minimal work. In contrast, young healthy adults commonly use initial trunk momentum to aid in rising [34, 49, 56]. This entails negative work as the hips extend against the trunk's forward momentum and therefore requires more positive work to stand. Consequently, younger adults would appear to spend more work than older adults to stand. This is surprising because younger adults are typically the benchmark for comparison against the elderly and thus expected to exhibit

behavior that optimizes energy expenditure.

To ascertain if there is an advantage to using momentum from sit-to-stand, we employ a simple chair rise model and test whether momentum usage requires excess work. We also determine what benefits the strategy might offer over other strategies that may be more stabilizing, requires little joint coordination, or avoids actuating particular joints. Previous models have also suggested that minimizing torque derivative cost is an important criterion to mimicking chair rise [50]. Therefore, chair rise strategies utilizing torque derivative costs, in addition to work are explored. We propose that some combination of a work cost and a torque derivative cost could reproduce important components of chair rise behaviors.

4.1 Chair Rise Model

We performed trajectory optimization on a simple, sagittal-plane, chair rise model. The model consisted of three rigid links connected by hinge joints, representing the shank, thigh, and trunk. The main mass is connected to the trunk, and knee torque and hip torque actuate the three-link system, leaving the ankle unactuated.

The optimization includes two distinct phases of chair rise, delineated by seat lift-off. The first phase starts from an initial static, sitting position, where only the trunk may move prior to seat-off. The second phase starts with seat-off and ends at rest in a vertical standing position. For some of the models, we explicitly simulate only the second phase and implicitly account for the work performed with the trunk motion of the first phase. Because the model has a massless shank and thigh, the equations of motion approach singularity near upright standing. Therefore acceleration trajectories, instead of torques, were used as optimization variables. The optimization parameters therefore include hip acceleration during trunk lean and knee and hip acceleration trajectories following seat-off. Each acceleration trajectory is represented by linear splines with ten control nodes. Time for trunk lean and time for trunk extension are also free parameters.

There are several constraints for the optimization. problem. The initial and final states both require the trunk to be vertical and the system at rest. The pelvis also cannot travel below its initial position, a chair constraint. Under Normal configuration, the initial sit state is -90 degrees in knee angle and hip angle. In the BOS under COM condition, the initial knee angle is -120 degrees, and hip angle is -60 degrees. Extension is defined as positive, and flexion as negative.

Several objective functions were used. To study energetic economy, mechanical work performed by the knee and hip joints during the trunk lean and extension phases was investigated:

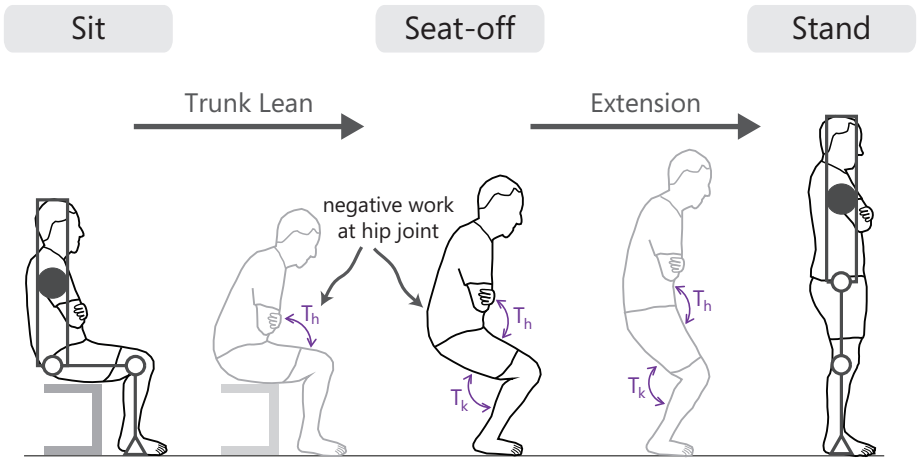

Figure 4.1: Three-link inverted pendulum chair rise model of sit-to-stand movement. The model is actuated by knee and hip torques. The simulation has two phases: trunk lean phase and extension phase, delineated by seat-off. Negative work could exist at the hip joint around seat-off.

$$J_{\text{work}} = W^{+}_{\text{hip OnSeat}} + \alpha W^{-}_{\text{hip OnSeat}} + |W_{\text{hip Rise}}| + |W_{\text{knee Rise}}| \tag{4.1}$$

where $\alpha \in \{-1,\ 0,\ 1\}$. If $\alpha = -1$, then the penalty for on-seat work is rectified work, and if $\alpha = 1$, then the model benefits from the return of negative work, similar to the use of a hip spring. When $\alpha = 1$, the work on the seat is equivalent to the sum of the trunk kinetic and potential energy at seat-off. Thus for these optimizations, only the extension phase was simulated. Since kinetic energy is positive and potential energy is negative, multiple solutions may exist for the trunk lean phase. Therefore, the minimum hip torque squared solution was used for this phase.

Work minimization is allowed to produce impulsive-like changes in torque trajectories, which seems unrealistic compared against human data [49]. Including a cost for force production adds smoothness to produce human-like forces [50, 55]. Therefore a torque-derivative cost function was used:

$$J_{\dot{T}} = \int \dot{T}^2_{\text{hip}} dt + \int \dot{T}^2{}_{\text{knee Rise}} dt \tag{4.2}$$

The trunk lean phase is only modelled by a single inverted pendulum representing the trunk. Therefore knee torque derivative costs during on-seat phase were not included in the cost function. The torque trajectory that minimizes this knee cost is a line from zero to the starting torque of the extension phase. While its biological implications are less clear, torque cost was also included for comparison:

$$J_T = \int T_{\text{hip}}^2 dt + \int T_{\text{knee}}^2 dt \tag{4.3}$$

To determine the influence of momentum, we also explored other chair rise methods and costs. Two strategies that do not use momentum include the BOS under COM strategy and No Momentum strategy. The BOS under COM strategy, as previously mentioned, starts in a different initial configuration from Normal and should only require knee torque and work to rise. For the No Momentum strategy, the trunk at seat-off is parallel to the thigh and has zero velocity. We also modeled a Hip Only strategy by minimizing knee torque cost.

4.2 Results

Different cost functions contributed to several strategies for chair rise. Work cost in terms of positive and negative work and torque costs consisting of knee and hip torque squared were calculated to compare the results. Amount of trunk lean and angular velocity at seat-off can indicate momentum usage. Minimizing work with $\alpha = -1$ gave different results from $\alpha = 1$ but did not differ from $\alpha = 0$. Minimum torque resulted in the lowest torque cost and comparable work cost to minimum work with $\alpha = -1$. Minimum torque derivative tended to the maximum allowable trunk lean and extension times and incurred the greatest torque cost. To avoid momentum, two possible chair rise strategies were to move the base of support under the center of mass such that the knees are no longer at a right angle (BOS under COM), or to have the trunk parallel to the thigh at seat-off (Without Momentum). BOS under COM used less work than the minimum work solutions but at the cost of greater knee torques. The Without Momentum had greater work and torque costs. A Hip Only solution was also found, and this solution also had high work and torque costs. Results from seven solutions are summarized with work and torque costs (Figure 4.2), cartoons of model simulations (Figure 4.3), and angle, torque, and power trajectories (Figure 4.4). Unless otherwise noted, angles are in degrees, and all other measures shown are normalized.

The minimal mechanical work objective found solutions that favored use of momentum and others that did not. When all of the hip's on-seat negative work can be utilized by the model ($\alpha = 1$), the trunk state at seat-off is at a greater angle than any other α conditions (-82 degrees) and at the slowest velocity (-0.0021). This results in a high hip torque cost and higher rectified work cost. When none of negative work is returned ($\alpha = 0$), the trunk angle is at -29 degrees and with higher velocity (-0.63). Knee torque cost is greater but hip torque lower, resulting in lower overall torque cost. Rectified work cost is also lower.

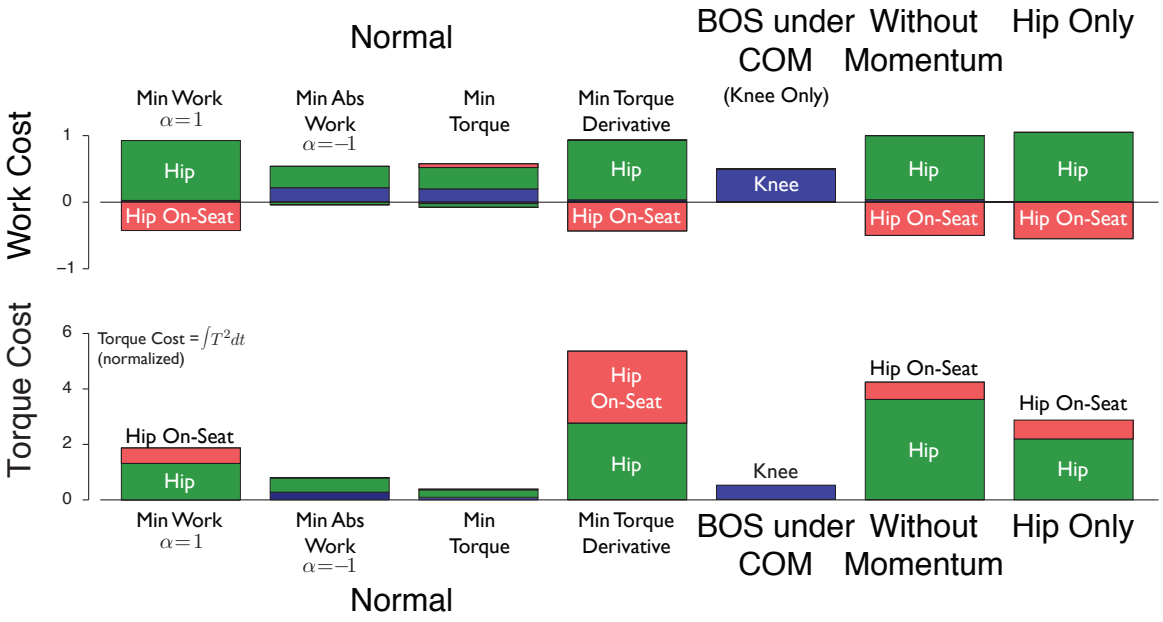

Figure 4.2: Work and torque cost of sit-to-stand movement under seven chair rise strategies. The lowest work cost occurs when the base of support remains under the center of mass and only knee extension is used to rise. The greatest rectified work cost occurs when only the hip is used to stand. Minimum torque cost strategy uses the lowest overall torque while the minimum torque derivative strategy has the highest torque cost.

When negative on-seat hip work is penalized ($\alpha = -1$), the results are similar to $\alpha = 0$.

Negative hip work was unavoidable. In the $\alpha = 1$ case, negative work was in the form of slowing the trunk down during the lean phase. Negative work was greatest in this situation because negative work offset the rectified work during the extension phase. However, in the $\alpha = 0$ case, negative work was used during the extension phase and resulted in overall less rectified work than the former condition. The following mechanical work cost functions gave identical results:

$$J_{\text{pos work}} = W^{+}_{\text{hip OnSeat}} + W^{+}_{\text{hip Rise}} + W^{+}_{\text{knee Rise}} \tag{4.4}$$

$$J_{\text{abs work}} = W^{+}_{\text{hip OnSeat}} + |W_{\text{hip Rise}}| + |W_{\text{knee Rise}}| \tag{4.5}$$

Note that Eqn 4.5 is equivalent to Eqn 4.1 when $\alpha = 0$.

Minimizing torque cost favored the use of momentum with the least trunk flexion (-20 degrees) and most angular velocity (-0.72) at seat-off. While an optimal solution existed for minimizing knee and hip torque cost during extension, minimizing hip torque cost during trunk lean produced the minimum solution only with infinite time. Most of the on-seat hip

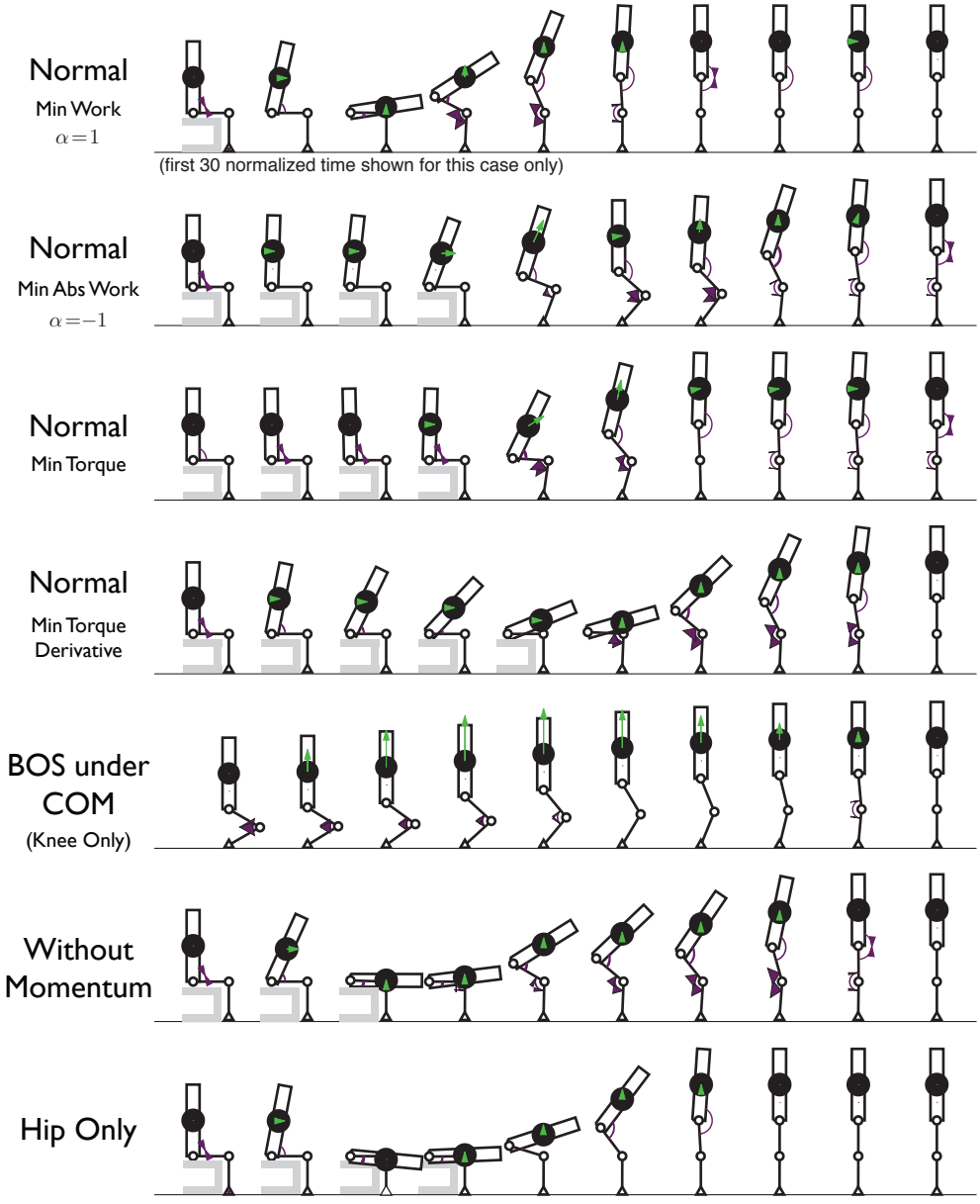

Figure 4.3: Ten frames of seven chair rise strategies. Cartoon indicates size and direction of knee and hip torques (purple) as well as the direction of the model's center of mass velocity (green). Only frames from the first 30 normalized time of Normal Min Work ($\alpha = 1$) are shown. All others are frames from the full simulation.

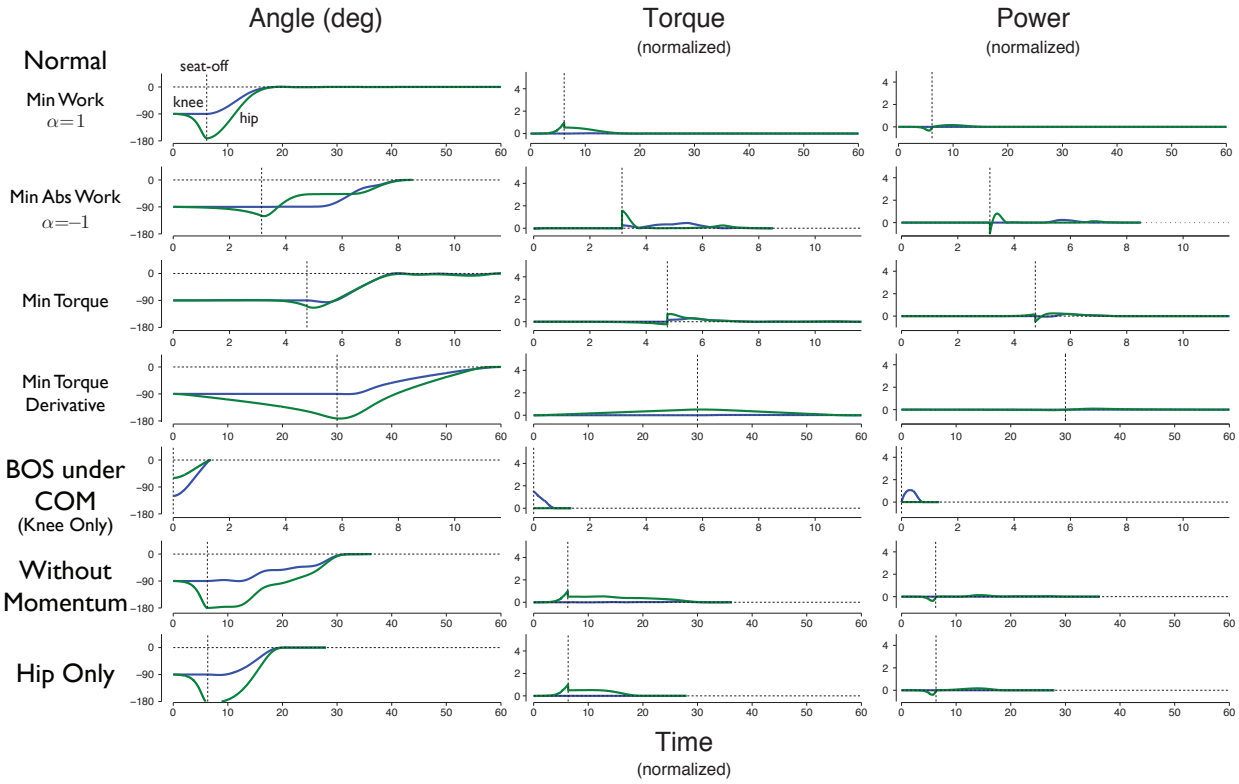

Figure 4.4: Knee and hip angle, torque, and power for seven chair rise strategies. Seat-off is indicated (dashed line). Minimum work ($\alpha = 1$) solution is longer than 60 normalized time, but the trajectories after 60 are near zero because the model is already standing at rest.

torque cost is incurred near seat-off to increase trunk velocity. However, prior to this, only infinitesimal application of torque in flexion is needed to initiate the trunk's descent due to gravity, given infinite time. Hence the hip torque cost during trunk lean is approximately the same after normalized time of 1 and is incrementally decreasing as time on seat increases. Here we present one solution with normalized time of 4.75 during trunk lean.

The solution that minimized torque derivative is smooth and tends towards using infinite time. Given an upper bound time constraint for the trunk lean and extension phases, the optimal solution will use the maximum time allocated. The solution shown is for a normalized time of 30 for trunk lean and 30 for extension phases (Figure 4.4). With this solution, the trunk at seat-off is at -82 degrees with an angular velocity of -0.024. Therefore the trunk has little momentum at seat-off despite the negative work during trunk lean. While the torque derivative solution may mimic the smoothness of human movement trajectories, it had the highest torque cost among all solutions and the third highest rectified work cost.

We compared the work and torque solutions against configurations that avoid momentum usage. One option for avoiding momentum is to start with the base of support directly under the center of mass. The cost function used for this configuration was minimum work with $\alpha = 1$. Since this cost function and configuration combination can produce a variety of solutions, depending on movement time, the BOS under COM result used here minimizes work as well as extension time and knee torque cost. While the optimization had the option to use the trunk, the optimal solution only used knee torques. This produced a solution with lowest amount of work at the cost of knee torque.

Another option for avoiding momentum without changing configuration is to place the center of mass over the base of support with trunk parallel to the thighs with zero angular velocity at seat-off. In this case, on-seat negative work serves to move the trunk towards the thighs, slowing down to zero velocity. This strategy has the second highest torque cost and second highest work cost.

We also simulated the strategy Hip Only, which only uses hip torque from sit-to-stand. This strategy is similar to No Momentum but incurs less torque cost. At seat-off, the trunk angle is -96 degrees and angular velocity is 0.0256. Hence, little trunk momentum is used at seat-off, perhaps because the model center of mass is already close to the base of support.

A chair rise strategy based on minimizing work and torque derivatives could mimic aspects of human chair rise movement. Minimal work strategy should expend the least energy, and minimizing torque derivatives should produce smooth torque trajectories. The combined cost function is:

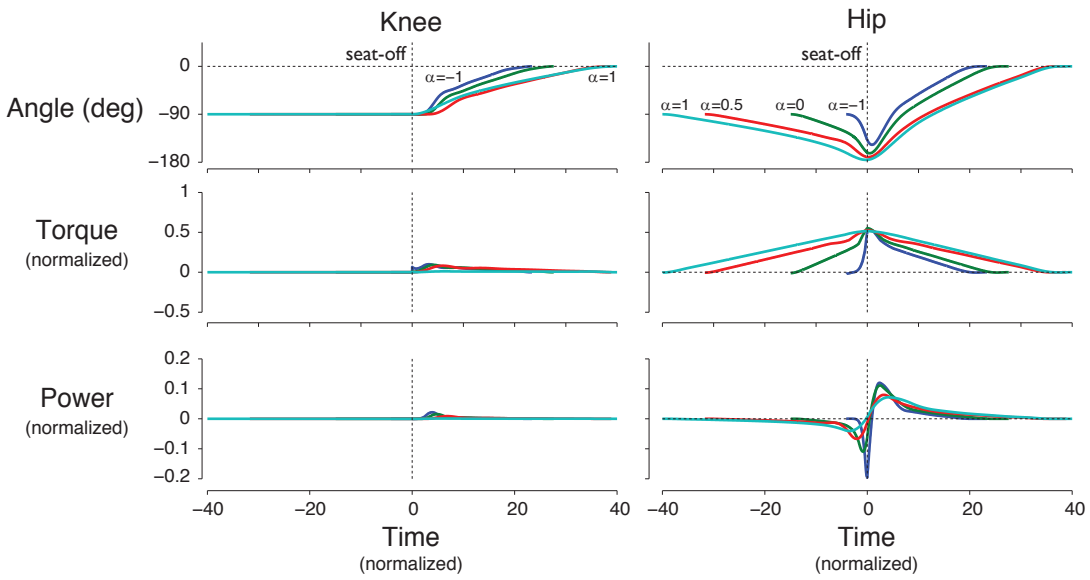

Figure 4.5: Knee and hip angle, torque, and power trajectories for solutions to combined work and torque derivative cost function for various α's. Trajectories are shifted in normalized time, such that seat-off occur at time 0. Solution with $\alpha = 1$ produces longest sit-to-stand duration and smoothest result while $\alpha = -1$ produces shortest movement duration with the least smooth trajectories. All solutions have similar maximum peak hip torque but differ in peak hip flexion and power.

$$J_{\text{combined}} = W^{+}_{\text{hip OnSeat}} + \alpha W^{-}_{\text{hip OnSeat}} + |W_{\text{hip Rise}}| + |W_{\text{knee Rise}}| + \int \dot{T}^2_{\text{hip}} dt + \int \dot{T}^2{}_{\text{knee Rise}} dt \tag{4.6}$$

When $\alpha = 1$, the solution tends towards infinite time, due to the influence of the torque derivative cost. The solution presented here is for normalized time of 40 for the on-seat and off-seat phases (Figure 4.5). This solution has the greatest trunk lean at seat-off (-86 degrees), which incurs negative hip work that reduces overall cost of J_{combined}. The solution also does not use momentum (0.0073 trunk velocity), similar to the minimum work only solution. At the other extreme, $\alpha = -1$, the torque trajectories are less smooth. However, momentum is utilized here as the trunk at seat-off has the least flexion (-48 degrees) but most trunk velocity (-0.3870). Hence there seems to be a tradeoff between amount of rectified work and level of smoothness (Figure 4.6).

We compared the optimal solutions to J_{combined} to human data. We qualitatively compared the solutions' model horizontal and vertical center of mass trajectories (Figure 4.7) to those found in Mathiyakom et. al [43] and Riley et. al [56] and hip angle trajectories from Schenkman et. al [60]. The solution with $\alpha = -1$ seems to the best fit human data.

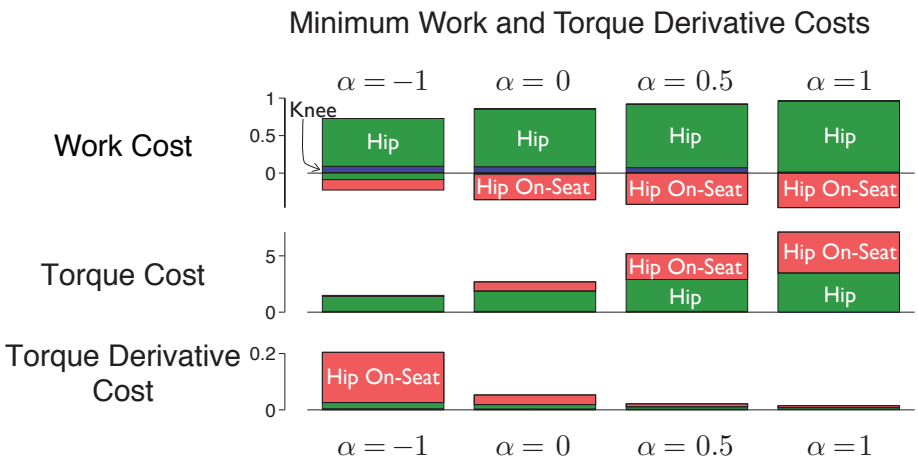

Figure 4.6: Work, torque, and torque derivative costs for the combined minimum work and torque derivative cost function. Rectified work and torque costs increase from $\alpha = -1$ to $\alpha = 1$ while torque derivative costs decrease.

The COM direction change from horizontal to vertical movement is gradual, as opposed to the sharp change for $\alpha = 1$. Maximum hip flexion angle is approximately -100 degrees for one human subject [60]. While all solutions' maximum hip flexion angles are greater, hip flexion angle $\alpha = -1$ is the closest to human data. Therefore, the most human-like trajectory, balancing rate of torque production and work, might occur somewhere between $\alpha = 0$ and $\alpha = -1$.

4.3 Discussion

We tested whether the minimum work solution used momentum. We also explored the consequences of rising without momentum and investigated whether a combined cost of work and torque derivative could reproduce human-like chair rise behavior. Some minimal work solutions used momentum ($\alpha = 0$, $\alpha = -1$) while others did not ($\alpha = 1$). Minimizing torque squared also utilized momentum while minimizing torque derivative did not. Both No Momentum and Hip Only strategies were similar and did not use momentum. Negative work was unavoidable in all cases except BOS under COM and acted to slow trunk velocity either prior to seat-off, which resulted in little forward trunk velocity, or shortly after seat-off, to redirect momentum. Overall, we found that momentum usage balanced the work performed by the knees and hips, as both joints share the load in lifting the body center of mass from sitting to standing.

We proposed that human-like optimal control might be obtained by minimizing work and the time-derivative of torque production. In contrast, Pandy's more extensive model

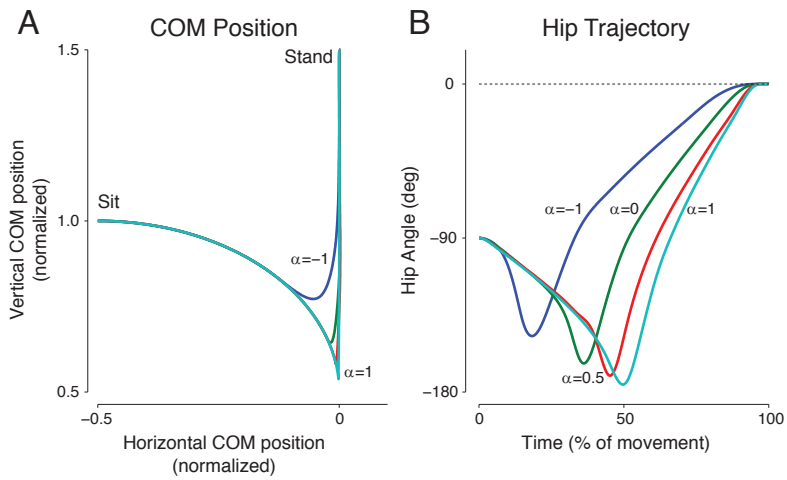

Figure 4.7: Vertical and horizontal COM position during sit-to-stand (A) and hip angle (B) for combined work and torque derivative costs. COM direction change from a mostly horizontal movement to vertical is smoother for $\alpha = -1$. Maximum hip flexion is also the least for $\alpha = -1$.

suggested that minimizing torque during trunk lean and torque derivative during extension best captures human chair rise movement [50]. Here we did not explicitly compare our torque results against human data, choosing to compare more biologically related costs. However, our results showed that the optimal solution to minimizing torque cost during trunk lean occurs with infinite time, and therefore suggesting that such a solution is unhuman-like. While the combined cost function was able to simulate some aspects of human behavior, not all behavior was captured. For example, the trunk flexion at seat-off was large and the movement less smooth than shown in human data. However, this simple model had no leg mass or ankle actuation, and thus a more complicated model may better fit human motion.

There are several limitations to this simple model of sit-to-stand movement. No chair was modeled and therefore any dynamical interactions between chair and model were not considered. Torque discontinuities at seat-off were also allowed, except for torque derivative solutions, which are infeasible for humans. However, this may be approximated by a fast torque change that occurs short timescales. The No Momentum condition at seat-off is only feasible when the center of mass can be placed over the base of support in the Normal configuration. Our model allowed this due to chosen segment lengths and the concentration of mass at the middle of the trunk. If the model is such that the center of mass always remains posterior to the base of support during trunk lean, then some amount of forward momentum is needed to stand. We also did not consider forces and torques, muscle activation, and movement duration in comparing model results to human data. Instead, we

compared COM and hip trajectories, which describe the overall chair rise motion.

The chair rise model can provide further understanding of compensation strategies, such as from lack of coordination or strength [61], and the consequences of such behaviors in older adults. For example, it is unclear from experimental studies of older adults if the use of momentum requires more or less knee torque and is more or less physically demanding overall [31, 59]. Our optimization showed strategies without momentum operate at the extremes, requiring the greatest knee torque and least hip torque or vice versa. We determined that momentum strategy balances both, suggesting that it may be the least demanding. Further model comparisons against human data are still needed. However, this simple model could help distinguish among chair rise strategies, highlight their advantages and disadvantages, and yield insights that are difficult or time-consuming to obtain from human studies.

CHAPTER 5

Determinants of preferred ground clearance during swing phase of walking

5.1 Introduction

The foot momentarily passes close to the ground about mid-way through each swing phase of walking. This instance also approximately marks the foot's peak speed over a stride, about three times walking speed [73]. This presents a risk of unexpected ground contact and susceptibility to tripping, stumbling, and even falling [3, 5]. Tripping is to be avoided, because it is one of the primary causes of falls for older adults [3], who incidentally tend to walk with reduced foot-ground clearance [4]. Clinical conditions such as drop-foot or weak hamstrings [13] can also lead to inadequate clearance, and thus compensations such as hip hiking and swing leg circumduction [13, 35] that also have negative consequences. Even healthy individuals avoid unwanted ground contact, for example on uneven terrain, by lifting the foot higher mid-swing [21]. Although all of these effects clearly favor greater ground clearance, that may also come with a cost, for example greater energy expenditure [70] that could be simply to lift the foot higher with each step. There may thus be two competing trade-offs: a cost for making inadvertent ground contact, and one for lifting the foot mid-swing. Together, these could explain the (non-zero) clearance humans normally prefer. We therefore seek to test the trade-offs between lifting the foot and allowing it to make contact with the ground.

There are several reasons why lifting the foot could be costly (Figure 5.1). For an otherwise normal gait, lifting the foot higher entails greater potential energy mid-swing, perhaps entailing more muscular effort. The effort might be reduced if elastic tendons of the leg and foot helped launch the foot into swing. This may already be the case normally, but any additional lift would entail more elastic energy, requiring more muscle force (in series with and supporting elastic tendon). Foot-to-ground clearance can also be examined with a model of

walking including the dynamics of the thigh and shank, mediated by elastic springs crossing the joints [15]. The model's passive dynamics can produce a human-like gait, where push-off from trailing leg and spring parameters, in the form of stiffnesses and moment arms, determine the swing foot's trajectory. Although such a model has no difficulty clearing the ground, it would also be able to maintain the same speed with lower push-off work and lower spring stiffness (and thus muscle force) if not for mid-swing ground contact, which causes the model to stumble [15, Figure 7]. The model could therefore be more economical if there were no ground to make contact with between footsteps. Of course, any model can only suggest how humans might behave, rather than provide a definitive answer. It is therefore important to test whether lifting the foot higher actually requires more mechanical work performed by the body, and whether there is also an increase in the metabolic cost for walking.

There are also likely costs to making ground contact mid-swing. As mentioned above, stumbling and falling are major concerns, which although relatively infrequent, could entail considerable pain, injury, gait recovery, and energy expenditure. Another, less important but more common, is occasional scuffing of the ground, which might go unnoticed if not for the wear on shoe soles. It is, however, difficult to compare mid-swing ground contact against lifting of the foot, because the motions are quite different, as are the types of costs they entail. One simplification is to treat the motions along a continuum of vertical ground clearance, with positive values signifying lifting the foot higher, and negative, striking the ground harder (as if the foot could drop through the floor if the latter were not there). As for the costs, a typical optimization approach is to consider multiple contributions [74], each weighted and summed to yield a single objective function, with arbitrary units. This also means that any units can be chosen, including those already used for foot lifting, namely metabolic cost. A remaining problem is that the costs of stumbling and falling are not straightforward to quantify in any units. However, the cost of even light scuffing of foot against ground, without stumbling or falling, could be considered a lower bound on the overall cost of unwanted ground contact, and can be quantified in terms of metabolic cost. If scuffing is costly, then the additional risk of stumbling and falling is only more so, and scuffing alone might be sufficient to favor greater ground clearance.

Another factor in the foot's motion is the notion of risk and probability (see probability distribution in Figure 5.1). If the foot were controlled with perfect precision, a ground clearance of zero might be optimal, because it would entail no excess effort to lift the foot, while also avoiding scuffing. But the actual foot motion is variable from step to step, and behaves according to a slightly skewed normal distribution, with a mean of about 1.56 cm and standard deviation of 0.62 cm [4]. In addition, on some terrains the smoothness of

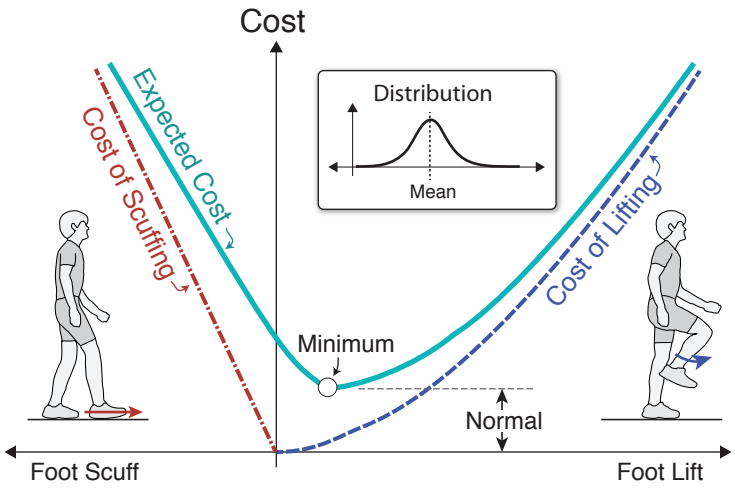

Figure 5.1: Proposed cost of ground clearance, in metabolic power, including separate contributions for scuffing the foot on the ground, for lifting the foot higher, and movement variability. Cost of scuffing is steeper than the cost of leg lifting near the origin. Therefore the cost of scuffing becomes less influential at some positive leg lift, resulting in a preferred cost at some positive foot lift.

the ground surface will also present variability, and occasionally cause negative ground clearance even when the foot would otherwise clear the ground. This risk can be accounted for using the expected value function from probability theory [7]. The expected value considers the both the probability distribution of the foot's motion and the costs for various mean clearances, to yield an overall probabilistic cost for ground clearance.

Here we investigate the energetic cost and biomechanical consequences of foot-to-ground clearance during swing. We propose that the preferred foot-to-ground clearance during walking is governed by interactions between two cost trade-offs, one for lifting the foot, and another for scuffing the foot due to negative foot lift, mediated by a probability distribution for the step-by-step variability of foot motion. Since much of gait appears to be energetically optimal, the preferred clearance height may closely match with the lowest metabolic cost. We expect that lifting the foot higher should require more mechanical work and come at greater metabolic cost. We also expect that negative foot lift, or greater amounts of scuffing should also require more effort and also lead to greater metabolic cost. These costs, along with the probability distribution of foot motion, may explain the preferred ground clearance during normal walking.

5.2 Experiment

We measured the costs of walking at different foot clearance heights performed by young, healthy adults. We used real-time visual feedback to enforce varying amounts of foot lift and scuffing during treadmill walking. We measured metabolic energy expenditure as the cost, and also characterized the associated gait kinematics and kinetics. Foot lift was characterized by the overall mechanical work performed on the body center of mass (COM) and by the joints, while scuffing was characterized by the horizontal impulse (time-integral of fore-aft force) produced by the foot against the ground surface during swing. Eight subjects (N=8, 1 female, 7 male) walked at varying levels of ground clearance during leg swing at a constant speed of 1.25 m/s on an instrumented treadmill. Subjects walked normally and with three levels of foot lifting and three levels of scuffing during swing phase of walking (Figure 5.2). The thresholds, termed Low, Medium, and High, to achieve during swing were 0.1 m, 0.2 m, and 0.3 m for foot lift and 100 N, 200 N, and 300 N for scuff force. Lift thresholds were measured from the treadmill surface, and scuff force was defined as aft-directed force produced by the foot, or equivalently the drag ground reaction force mid-swing. One subject's scuffing data was excluded because they were found to scuff smoothly into heel strike instead of during mid-swing, making the scuff impulse indistinguishable from normal heel contact. Subject received visual feedback of toe marker height during foot lift conditions, and fore-aft ground reaction force during scuffing conditions. In each case, these were displayed in real time along with a target threshold for either scuff force or lift height. Trials were performed in randomized order, and were of 6 minutes in duration. Subjects' age ranged from 18 to 29 years, and their body mass M was 73.8$\pm$11.1 kg (mean$\pm$SD) and leg length L was 0.93$\pm$0.05 m. All subjects provided written informed consent prior to the study, according to Institutional Review Board procedures.

We measured metabolic power and gait mechanics using standard procedures. Net metabolic rate (in W) was estimated from the rate of oxygen consumption and carbon dioxide production using standard conversion factors [10]. Steady-state metabolic power was averaged over the last 2 minutes of each 6-minute trial, and the rate for quiet standing (99.2$\pm$17.1 W, 0.0467$\pm$0.0123 dimensionless) subtracted from the gross rate to yield net metabolic power. Kinematic and kinetic data were also recorded over the same time with motion capture (PhaseSpace, San Leandro, CA USA), using a modified 24 marker set [76]. Lift Height z_{LH} for the foot was measured as the maximum vertical height of the toe marker (fifth metatarsal) during swing, minus its height during quiet standing. Scuffing was measured with the Scuff Impulse $\hat{F}_{\mathrm{SI}}$, defined as the integral of fore-aft ground reac-

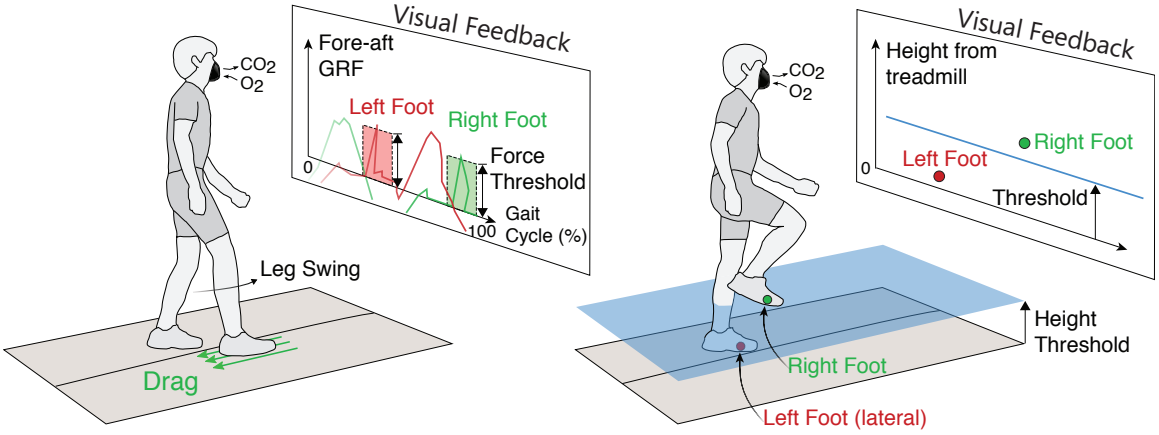

Figure 5.2: Subjects walked with varying levels of foot lift and scuff force on a split-belt treadmill at 1.25 m/s. During scuffing conditions, subjects had to produce a drag, or aft, ground reaction force during swing phase walking, indicated by two boxes, one for each leg. In the foot lift conditions, subjects' lateral toe marker had to clear a virtual bar with each step. Visual feedback enforced subject compliance to foot lift or scuff thresholds.

tion force during the swing phase, normally zero when there is no scuffing. As a point of comparison, we calculated the average total horizontal drag impulse generated per stride for normal walking C_{Drag} (26.2$\pm$4.32 N-s). Also measured was the rate of work performed on the COM, termed instantaneous COM work rate [17], computed as the inner product of the ground reaction forces of each leg and the COM velocity. Standard kinematics and inverse dynamics procedures (Visual3D, C-Motion, Germantown, MD, USA) yielded ankle, knee, and hip angles, and joint moments and powers. As a simple summary of joint work, we defined summed joint power as the net power from ankle, knee, and hip of one leg. Average positive COM and summed joint work rates for both sides of the body were calculated from the positive work per stride divided by stride time and multiplied by 2. The same computation was performed for negative work rates. Finally, step lengths and widths were also computed, along with root-mean-square variabilities, for each trial.

We expected that the increasing levels of each condition would affect the corresponding measure and metabolic cost. Thus, Scuff Impulse was expected to increase with scuff condition, and Lift Height increasing levels of the foot lifting condition. We also tested for simple relationships between these measures and metabolic rate. For scuffing, we performed a linear fit between scuff impulse $\hat{F}_{\text{SI}}$ and net metabolic rate $\dot{E}_{\text{SI}}$. For foot lift, we tested for a quadratically increasing cost $\dot{E}_{\text{LH}}$ with Lift Height z_{LH}, based on an assumption of an even function. However, the shape of this function is difficult to predict, and so we also tested for a linear relationship. Fits were performed for all of the data from each condition simultaneously, allowing each subject to have an individual constant offset. Sta-

tistical tests were performed on the coefficients, with a significance level of $\alpha = 0.05$. The effect of each condition on corresponding measures (C_{SI} and z_{LH}) was also tested (ANOVA followed by post-hoc t-tests with Holm-Sidak correction for multiple comparisons, [22]).

Dimensionless measurements are reported here, using the base units of body mass M, standing leg length L, and gravitational acceleration g. Force was normalized by Mg (mean 723.6 N), moment and work by MgL (mean 670.8 Nm), power by $Mg^{1.5}L^{0.5}$ (mean 2182 W), step length and width by L (mean 0.9265 m), and step time by $\sqrt{L/g}$ (mean 0.3072 s).

5.3 Ground Clearance Cost Model

We measured two main contributions to foot-ground clearance: a cost for foot lift, a cost for scuffing the foot, as well as clearance variability during swing of Normal Walking (Figure 5.1). We propose a linear cost function for scuffing. Scuffing cost should increase with greater drag force produced by the ground at foot-to-ground contact. However, if instead the ground provided an assistive force to move the swing leg forward, hypothetically the cost should decrease. Thus a linear function, the simplest odd function, could model cost of scuffing. For the cost of foot lift, it seems costly to both lift the legs and to extend the legs past nominal. Therefore an even function, such as a quadratic function, was used to model cost of foot lift. We propose that the cost of scuffing and cost of foot lift both contribute to the expected cost of ground clearance through probability distribution of achieving a certain ground clearance. The expected cost of ground clearance $\dot{E}$ is:

$$\dot{E}(x) = \int (C_{\text{SI}} + C_{\text{LH}}) p(w, x) dw \tag{5.1}$$

where C_{SI} is the cost of scuffing, C_{LH} is the cost of foot lifting, and $p(w, x)$ is the probability density function centered around some ground clearance x. Near the origin, the cost of scuffing is steeper than the cost of foot lifting. Therefore the cost model yields an expected preferred cost that is shifted towards positive foot lift. We test if the human ground clearance data could match the proposed cost of foot lift and cost of scuffing models.

5.4 Results

We found each of the experimental conditions to yield different levels of the corresponding measures for scuff impulse or lift height (Figure 5.4). The conditions also resulted in substantial changes in metabolic energy expenditure, as well as with alterations

	Lift Height		Scuff Impulse		Net Metabolic Rate	
	SI	dimensionless	SI	dimensionless	SI	dimensionless
Normal	0.0886±0.0146	0.0956±0.0144	-0.0273±0.0518	-1.264e-4±2.417e-4	176.93±32.357	0.0833±0.0228
Lift Low	0.1436±0.0293*	0.1553±0.0325*	-0.0565±0.0557	-2.462e-4±2.385e-4	254.96±67.680*	0.1204±0.0399*
Lift Medium	0.2236±0.0147*	0.2416±0.0150*	-0.0320±0.1335	-8.451e-5±6.874e-8	325.08±94.062*	0.1527±0.0503*
Lift Height	0.3018±0.0330*	0.3259±0.0321*	-0.1044±0.1371	-4.490e-4±5.833e-4	411.27±114.818*	0.1920±0.0572*
Scuff Low	0.0823±0.0154	0.0888±0.0154	0.7736±0.2669*	0.0037±0.0016*	223.27±66.037*	0.1074±0.0313*
Scuff Medium	0.0861±0.0185	0.0861±0.0185	1.4229±0.3006*	0.0067±0.0015*	290.30±64.790*	0.1394±0.0314*
Scuff High	0.0804±0.0219	0.0867±0.0231	2.1282±0.4629*	0.0102±0.0033*	339.34±88.586*	0.1650±0.0503*

Table 5.1: Lift height, scuff impulse, and net metabolic rates in both dimensional SI units and dimensionless form (mean ± SD). Statistical significance (*) compared against Normal indicated if $P < 0.05$.

to gait biomechanics. Net metabolic rate increased quadratically with increasing lift height (treated as a continuous variable), and linearly with scuff impulse (also as a continuous variable). Positive and negative joint and COM work rate also increased with greater foot lift. In contrast, foot scuffing had less obvious effect on biomechanical measures despite its relatively high energetic cost. The main findings are detailed below (see Table 5.2 for quantitative results for step parameters, work, and work rate measures).

Significant changes were produced by each of the discrete walking conditions for foot scuffing and lifting (Figure 5.4, Table 5.1). These were observable in the form of aft-directed ground reaction forces for scuffing and higher foot trajectories for lifting, summarized by significant changes in scuff impulse $\hat{F}_{\mathrm{SI}}$ and lift height z_{LH}, respectively (all $P < 0.05$). The scuffing conditions resulted in aft-directed impulses up to $2.13 \pm 0.46\,\mathrm{N \cdot s}$ for the High condition, equivalent to about 8.6% the aft-directed impulse for an entire normal stride. The lifting conditions resulted in heights about 1.62 to 3.41 times greater than the normal lift of $0.0886\,\mathrm{m}$.

As expected, the preferred, normal lift height approximately coincided with minimum metabolic cost (Figure 5.4). Net metabolic rate increased for greater magnitude of lift height or scuff impulse, treating the two measures as continuous variables. There was an approximate linear trend for scuff impulse, with slope -7.03 ± 1.99 (mean ± c.i., 95% confidence interval) and offset 0.088 ± 0.0316 (mean ± s.d.), equivalent to about -68.9 W/N-s and 183 W, respectively, with $R^2 = 0.748$ ($p = 3.95\mathrm{E}-7$). There was also a significant trend for lift height with quadratic coefficient 0.9876 ± 0.2363 and offset 0.0877 ± 0.0409 (equivalent to about $2517\,\mathrm{W \cdot m^{-2}}$ and $185\,\mathrm{W}$, respectively) with $R^2 = 0.77$ ($p = 1.10\mathrm{E}-8$). Lift height also produced a significant trend with linear coefficient 0.4395 ± 0.0928 and offset 0.0472 ± 0.0410. As a simple indicator, dragging the foot with impulse 11% of the normal aft-directed ground reaction impulse caused an approximate doubling of metabolic cost. A similar doubling of cost resulted from lifting the foot about $23\,\mathrm{cm}$ higher than Normal. Minimum clearance during normal walking, as measured from

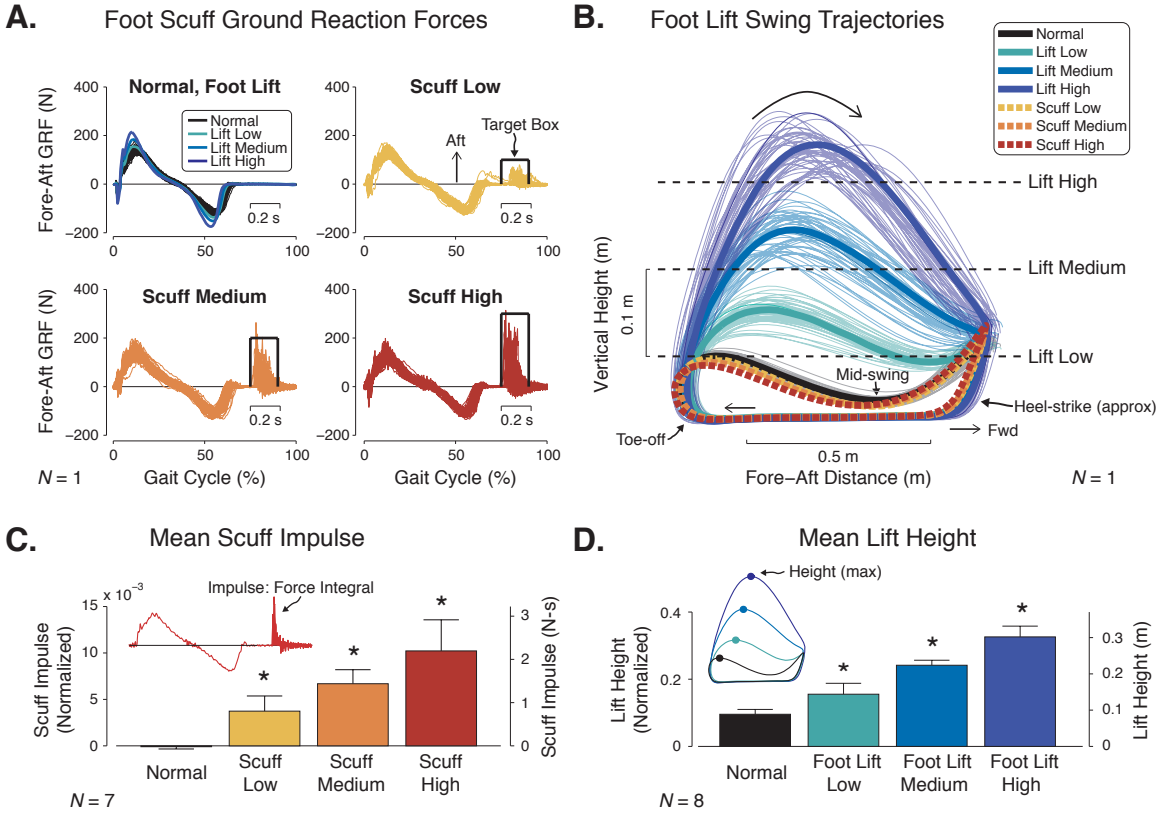

Figure 5.3: Measures of scuffing and foot lift observed in experimental conditions. (A) Fore-aft ground reaction forces from a representative subject ($N = 1$) indicate greater drag (aft) force achieved from low to high scuff threshold levels (solid rectangle). None to negligible amounts of scuffing occurs with Normal or Lift conditions. (B) Fore-aft and vertical trajectory of the lateral toe marker from a representative subject ($N = 1$) for various lift height thresholds from the treadmill. Mean ground clearance levels achieved by subjects measured through (C) scuff impulse ($N = 7$) and (D) lift height ($N = 8$). All levels of ground clearance were significantly different from normal ($P < 0.05$). Left-hand axes are dimensionless, using body mass, leg length, and gravitational acceleration as base units; right-hand axes are SI units.

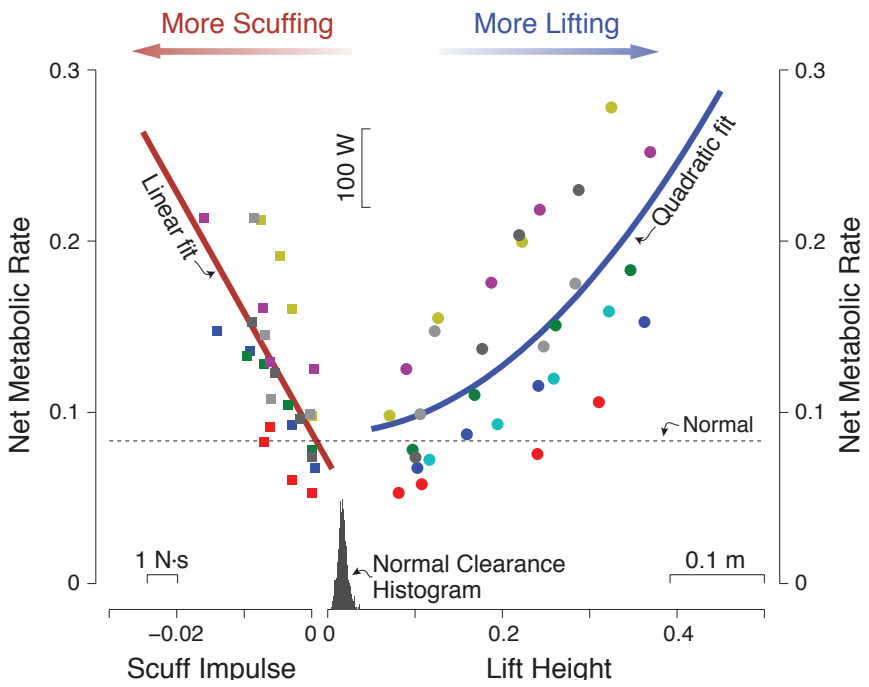

Figure 5.4: Net metabolic cost as a function of measured scuff impulse (left) and lift height (right). Net metabolic rate increased with greater scuff impulse ($N = 7$) at a rate of -68.9 W/N-s ($R^2 = 0.75$, $P < 0.05$) and with greater lift height ($N = 8$) at 2517 $\mathrm{W \cdot m^{-2}}$ ($R^2 = 0.77$, $P < 0.05$). Distribution of minimum toe clearance during swing indicates movement variability during normal walking. Separate colors denote each subjects' data (square for scuffing, circle for foot lift). Mean net metabolic cost for normal walking also indicated (dashed). Net metabolic rate defined as gross metabolic rate minus quiet standing rate. Metabolic rate, scuff impulse, and lift height are in dimensionless units, using body mass, leg length, and gravitational acceleration as base units.

the trough of the marker trajectory, was 0.0157 $\pm$ 0.0046 m.

There were changes in step parameters for leg lift but not for scuffing (Table 5.2). Subjects exhibited longer step length, step width, and step period and shorter double support duration with increasing lift height (0.53 m longer, 0.17 m wider, and 0.43 s more time, and -0.11 s more time, for each 1 m of additional lift height, respectively; all $P < 0.05$). There were also small increases in step length and width RMS variability (0.0504 m and 0.0588 m per 1 m lift, respectively, $P < 0.05$). However, the only changes in step parameters were slightly increased step width and step length variability (-0.0088 m and -0.0034 m per 1 N-s additional scuff impulse, respectively, $P < 0.05$).

Foot lifting appeared to have greater effect on the mechanics of walking than scuffing. Qualitatively examining force and power trajectories (Figure 5.5), greater foot lift appeared to magnify the first peak of the vertical ground reaction force (GRF), the positive and negative peaks of the fore-aft GRF, and the magnitudes of COM and summed joint power. In

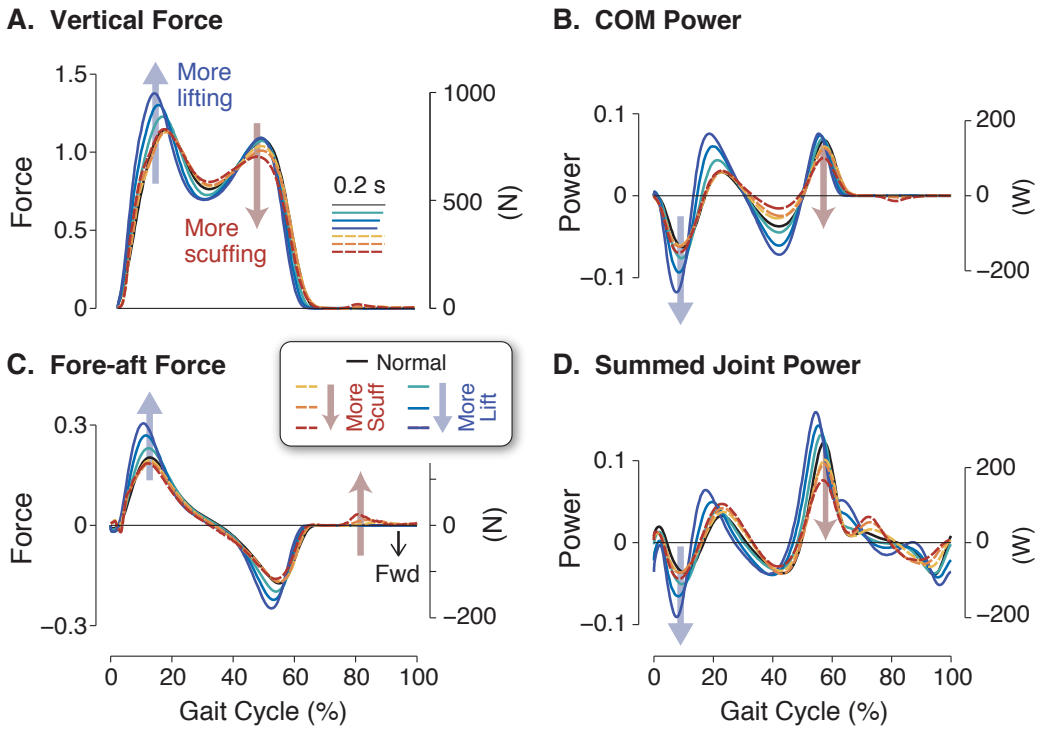

Figure 5.5: Force and power measures versus time within gait cycle (% of stride) for varying levels of ground clearance (black for normal, solid for foot lift, dashed for scuff). Vertical and fore-aft ground reaction force, center of mass (COM) power, and summed joint power from sum of ankle, knee, and hip power from one leg. More qualitative changes are observed in lift conditions than in scuff conditions, compared against Normal.

contrast, scuffing seemed to have much less effect, perhaps slightly reducing the second peak of the vertical GRF and push-off power. In terms of joint kinematics (Figure 5.6), lifting the foot appeared to require more flexion in knee and hip during swing, while scuffing produced relatively minor changes. Lift height also produced changes in joint powers while only ankle push-off seemed to reduce for scuffing.

These observations are supported by quantitative differences in the work performed by the body (see Fig. 5.7). Scuffing resulted in only minor or non-significant changes in average work rates on the COM and by the summed joints, whereas foot lifting resulted in much greater and significant increases in work (see Table 5.2 for details and individual joint results). In particular, greater foot lift entailed more positive and negative work on the COM and by the joints, particularly the ankle and knee for positive work, and hip for negative work.

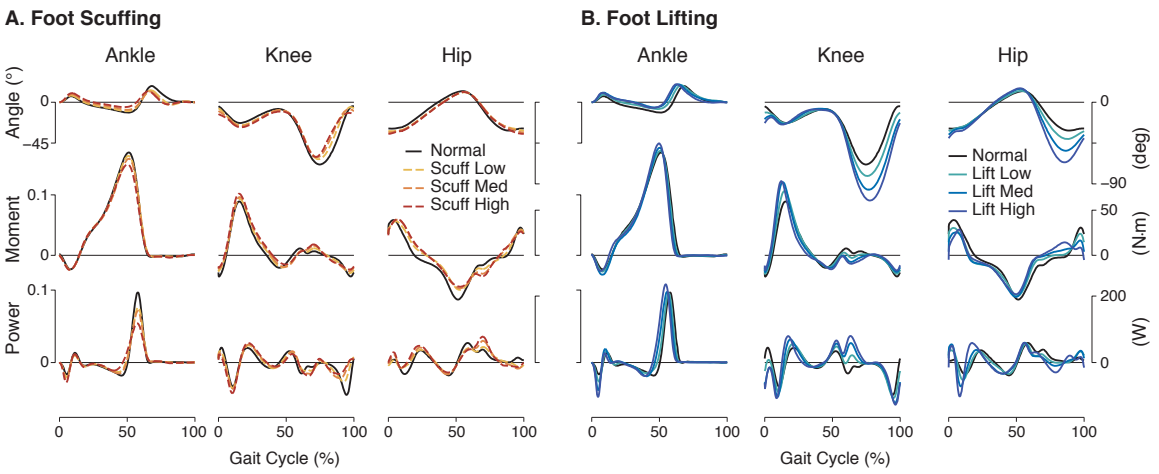

Figure 5.6: Joint angle, moment, and power for (A) foot scuff and (B) foot lift conditions. Trajectories vs. time for ankle, knee, and hip, with gait cycle starting at heelstrike. Left-hand axes are in dimensionless units, and right-hand axes are SI units.

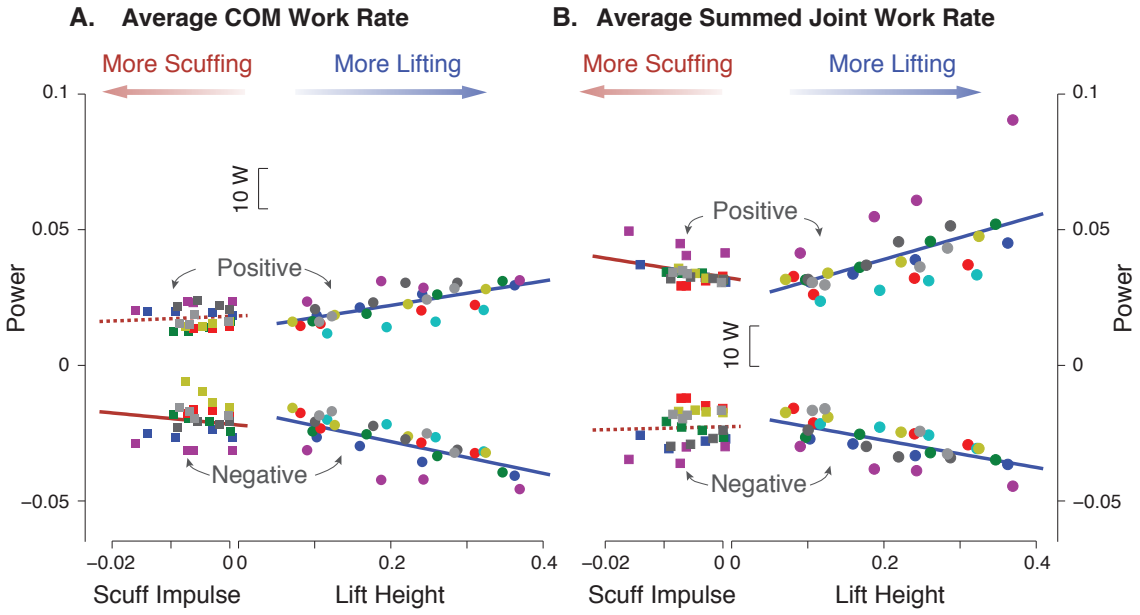

Figure 5.7: Mean positive and negative (A) COM work rate per stride and (B) summed joint work per stride against scuff impulse and lift height. Joint work rates include ankle, knee, and hip. Lift height had a greater impact on work rate than scuff impulse. Greater lift contributed towards significant increases in positive and negative COM work rate and joint work rate. However, scuff impulse only affected negative COM work and positive joint work rates, both at lesser rates than for lift height. Separate colors denote each subjects' data (square for scuffing, circle for foot lift). Trend significance ($P < 0.05$, solid line) and non-significance (dashed line) indicated.

	Lift Height				Scuff Impulse			
	Slope (mean±CI)	Offset (mean ± SD)	R^2	P	Slope (mean±CI)	Offset (mean ± SD)	R^2	P
Net metabolic rate	0.9876±0.2363	0.0877±0.0409	0.7707	1.1e-8*	-7.0388±1.9864	0.0881±0.0316	0.7475	4.0e-7*
Step length	0.5319±0.1585	0.7032±0.0580	0.6873	4.5e-7*	-1.0911±3.0302	0.7479±0.0576	0.0297	0.46
Step width	0.1733±0.0823	0.1532±0.0215	0.4598	2.3e-4*	-2.1181±1.0521	0.1663±0.0248	0.4893	4.4e-4*
Step length RMS	0.0504±0.0205	0.0148±0.0083	0.5367	3.8e-5*	-0.8175±0.6207	0.0218±0.0079	0.2908	0.012*
Step width RMS	0.0588±0.0196	0.0181±0.0070	0.6338	2.4e-6*	-0.2118±0.4866	0.0238±0.0065	0.0428	0.37
Step period	1.2822±0.3793	1.6959±0.1539	0.6869	4.0e-7*	-2.6384±7.2691	1.8043±0.1548	0.0302	0.46
Double support duration	-0.3217±0.0890	0.5539±0.0203	0.7148	1.3e-7*	0.3518±2.0775	0.5432±0.0147	0.0067	0.73
COM work (pos.)	0.1178±0.0239	0.0200±0.0076	0.8231	5.4e-10*	0.0850±0.2843	0.0325±0.0068	0.0207	0.54
COM work (neg.)	-0.1518±0.0239	-0.0248±0.0080	0.8854	3.6e-12*	-0.3095±0.3977	-0.0390±0.0108	0.1252	0.12
COM work rate (pos.)	0.0448±0.0076	0.0131±0.0041	0.8685	1.8e-11*	0.0874±0.1214	0.0181±0.0038	0.1093	0.15
COM work rate (neg.)	-0.0585±0.0078	-0.0164±0.0053	0.9151	1.1e-13*	-0.2079±0.1955	-0.0217±0.0065	0.2110	0.038*
Joint work (pos.)	0.2018±0.0394	0.0358±0.0136	0.8344	2.5e-10*	-0.7226±0.4046	0.0587±0.0056	0.4299	0.0013*
Joint work (neg.)	-0.1335±0.0236	-0.0276±0.0079	0.8601	3.6e-11*	0.1598±0.4520	-0.0408±0.0115	0.0287	0.4693
Joint work rate (pos.)	0.0802±0.0217	0.0230±0.0096	0.7241	9.2e-8*	-0.3471±0.1585	0.0326±0.0041	0.5315	1.9e-4*
Joint work rate (neg.)	-0.0501±0.0084	-0.0176±0.0049	0.8719	1.3e-11*	0.0530±0.2150	-0.0226±0.0068	0.0142	0.61
Ankle work (pos.)	0.0659±0.0271	0.0258±0.0095	0.5321	4.3e-5*	0.4780±0.5282	0.0335±0.0102	0.1622	0.0737
Ankle work (neg.)	-0.0272±0.0107	-0.0125±0.0043	0.5512	2.6e-5*	0.2016±0.2246	-0.0157±0.0037	0.1600	0.0759
Knee work (pos.)	0.1053±0.0160	0.0059±0.0098	0.8933	1.6e-12*	-0.5130±0.3447	0.0177±0.0084	0.3436	0.0056*
Knee work (neg.)	-0.0479±0.0197	-0.0264±0.0030	0.5305	4.4e-5*	0.2234±0.3180	-0.0299±0.0053	0.1045	0.1583
Hip work (pos.)	0.0438±0.0349	0.0209±0.0144	0.2323	0.016*	-1.3926±0.4001	0.0247±0.0086	0.7412	5.0e-7*
Hip work (neg.)	-0.0717±0.0180	-0.0054±0.0101	0.7534	2.5e-8*	0.4399±0.2541	-0.0125±0.0083	0.4147	0.0017*

Table 5.2: Dimensionless quantitative results for fits to metabolic rate, step parameters, and work and work rate as a function of lift height and scuff impulse. Fit parameters include trend value (means ± 95% CI) and offsets (means ± SD). R^2 values indicate goodness of fit, and P-values indicate statistical significance of the trend ($*P < 0.05$).

5.5 Discussion

We tested whether increased amounts of foot lift and scuffing would incur greater metabolic cost. Both were energetically costlier than preferred walking and increase with greater amounts of lift height or scuff impulse. The cost of scuffing fits a linear function, and the cost of foot lift fits a quadratic function. Therefore the slope of scuffing cost is steeper than the cost of foot lifting near the origin. Measurement of minimum toe height during swing phase of normal walking demonstrated variability in clearance movements. Hence, humans appear to compromise between cost of lift work and to overcome friction at foot-to-ground contact during swing. These tradeoffs are influenced by the uncertainty in clearance movements. The steeper influence of scuffing results in a preferred clearance at a positive lift height.

While both foot lift and scuffing were energetically costly, their biomechanical effects on gait differed. The greater foot lift cost could be attributed to changes in step parameters and to the mechanical work of lifting and lowering the foot. Greater foot lift requires more time, which, at a fixed speed, necessitates a longer step and shorter double support duration. Increased positive work was needed to lift the foot, and negative work was needed to slow the foot as it neared the ground. However, the contributions of scuffing mechanics were less clear. Scuffing only affected negative COM work rate and positive joint work rate. Scuffing also produced no significant changes in work done on the COM, but did require increased positive and negative joint work. The lack of changes in COM work could mean that producing a scuff impulse during swing did not require compensation from the stance leg, nor did it affect the work done on the COM. The swing leg itself through knee and hip provided the work for imparting a force onto the ground. Despite inducing a significant metabolic cost, scuffing has less identifiable costs due to traditional gait measures of gait. Perhaps the cost of rapidly producing a force for a short duration during swing or muscle co-contraction to hold against friction could explain the cost of scuffing.

The tradeoff between foot lift and scuffing can be facilitated by using the same independent variable for comparison. Using lift height as the independent variable, for example, lift height increased with greater scuffing within a small range, resulting in a much sharper increase in metabolic cost than with foot lifting. Using scuff impulse as the independent variable did not seem meaningful because the foot lift trials resulted in no contact with the treadmill and therefore no scuff impulse apart from fluctuations in treadmill noise. Here the tradeoff between scuff impulse and lift height was established by converting both into work measures using approximations for foot velocity and the mass lifted during swing, respectively. Work to produce a scuff impulse W_{SI} is calculated from product of scuff im-

pulse and foot velocity during swing. During mid-swing, the foot velocity is approximately three times the velocity of the body COM [73]. Therefore, the foot speed used was 3.75 m/s, three times the treadmill speed and therefore average COM speed. The lift work W_{TC} is the product of lift height, lift mass (swing leg), and gravity. Although various amounts of leg mass may be lifted depending on lift height, the mass used for lift work was the mass of one leg, $0.161M$ [72]. The metabolic costs and work rates presented previously are scaled such that both were plotted against scuff work and lift work measures (Figure 5.4, Figure 5.7). The cost of scuffing was steeper than that of foot lift, whether foot lift was fit by a quadratic or linear function. Another method to unify scuff and foot lift measures is to use measured positive joint work. This also resulted in a steeper cost of scuffing than foot lift. Hence while multiple methods may exist to convert scuff impulse and lift height to comparable units, scuffing seems to be costlier than foot lifting.

We did not consider the effect of treadmill speed on the cost of ground clearance. Studies have shown that preferred toe clearance increases with walking speed [14, 62]. The cost of scuffing and cost of foot lift would likely be steeper due to speed, but this suggests either the relationship between the two curves would remain the same or that scuffing would increase at a steeper rate than foot lift. It is also unclear what would happen at very slow speeds. For example, humans tend to scuff while walking when fatigued, perhaps because foot swing may be slowed by frictional drag without need for negative work. Hence the cost of scuffing may become less steep. However, one study showed that fatigue did not affect obstacle clearance heights compared against rested condition [26]. In addition, older adults, who tend to walk at slower speeds, had lower but not significantly different preferred height than young adults [4].

The proposed clearance cost model demonstrates that the cost of scuffing and cost of foot lifting both influence the preferred ground clearance due to movement variability. Several other costs that may contribute are not considered here. For example, the subjects scuffed intentionally during the experiment, and therefore the cost of scuffing due to accidental ground contact was not captured. If the scuffing was unplanned, cost of fear, cost of injury, and cost of recovery could contribute. Likewise, the foot lift thresholds were virtual. If actual obstacles were used with an implicit threat of accidental scuffing, other costs may factor into the cost of ground clearance. The consequences of unplanned ground contact would likely contribute towards a much steeper scuffing cost. However, use of virtual obstacles allows us to study foot lift and scuff as independently from each other as possible, and intentional scuffing may yield a lower bound on the cost of scuffing.

This cost model can make several predictions. For example, the model suggests that walking on uneven terrain, which shifts the cost of scuffing towards the right, will result

in a higher preferred foot lift. This seems to correlate with studies on walking on irregular surfaces and rocky terrain [21, 62]. The model also indicates that walking with greater swing variability, a wider probability distribution, will also result in greater foot lift. While normal walking produced the lowest measured energetic cost, the model predicts that a lower metabolic cost could hypothetically be achieved without ground interference during swing. This requires either stepping stones to allow for foot clearance without knee flexion during swing or shoe soles that provide frictionless interaction with the ground during swing but not stance.

CHAPTER 6

Discussion and Conclusion

The underlying theme in the previous four chapters is the use of controls theory in simple, mechanistic models to understand human behavior. I used this framework to investigate four essential activities of daily living: integration of sensory information, balance on one-leg, sit-to-stand movements, and maintaining ground clearance during swing phase of walking. The estimator model of sensory integration is mathematically parallel to the feedback model of one-legged lateral balance. The chair rise movement exemplifies feedforward control with some optimization of work and force production. The preferred foot-to-ground clearance is another optimization, as an energetic cost trade-off of two costly functions modulated by variability.

However useful a model, at some point its utility breaks down. Nonlinear dynamical effects or cognitive influences may influence human behavior but are not accounted for by simple models. For example, vection, the illusion of self-motion, has been shown to cycle on and off during a constant visual stimulus [65]. In addition, fear of falling has been associated with postural performance in the elderly [42] and Parkinson's patients [1]. Hence, risk-taking subjects may outperform risk-adverse subjects in one-legged balance tasks, even if both used similar balance strategies. Nonetheless, while many variables contribute towards human behavior, simple models serve as a baseline to consider a range of possible behaviors.

Simple models also may be easier for a wider audience across multiple disciplines to understand. A more complicated model may be able to reproduce a greater amount of postural responses, but the components that caused these responses are less clear. Complex models may also be less likely to be reproducible by the scientific community, and a lack of understanding could lead to misuse of the model findings. Perhaps the complexity of the models should be relevant to the aim of the investigation. If the goal is to reproduce detailed or fringe behavior, complexity can be added. However, for bulk behavior, such as postural responses about some operating point, simple models may serve to capture the overall behavior best.

6.1 Implications for Clinical Research

Simple controls models are useful for their ability to make predictions. With the estimator model, one can simulate how sensory degradation might affect postural response and test these predictions with data from older adults or vestibulopathic subjects, for example. Balance strategies may also change with age or disease, and stance leg gains during one-legged balance could demonstrate how limb prioritization differs from healthy adults. Bounds on limb torques to simulate muscle weakness, for instance, could reveal compensation strategies or reasons for balance failures by studying overall gain or gains of individual limbs. Simple model of chair rise movement can demonstrate how one strategy may be advantageous or detrimental over another. The ground clearance model can predict how the expected clearance may change depending on the ground conditions and amount of foot control. Hence normal and abnormal postural behavior under ordinary and novel environments can be better quantified and understood.

A divide seems to exist between postural research and clinical utility. Often clinical research qualitatively documents abnormal behavior, and sometimes the reason underlying such behavior may be apparent from a comparison between healthy and patient populations. However, simple models can bridge this divide by serving as a diagnostic tool to further facilitate understanding and provide intervention procedures. For example, balance assessment using one-legged balance may simply require counting how long the patient can balance [6, 8, 66]. However, duration may not necessarily determine why the patient cannot balance or how he or she fails to balance. Hence, knowledge of the feedback gain matrix could help answer these questions. Similarly, a common clinical test is to count the number of sit-to-stand movements performed by a patient within a given time. However, the differentiating factor between rising more or less times than a healthy individual is unclear. Here investigations of movement strategies, such as trunk lean and velocity at seat-off, may indicate why a patient may be limited in the frequency of their movements.

6.2 Implications for Balance and Control of Bipedal Robots

Understanding human behavior may provide insights into the balance and control of bipedal robots. These robots, like humans, are inherently unstable due to inverted pendulum-like behavior. As robots tend towards more dynamic, human-like behavior, the body center of mass may frequently venture outside of the base of support and require more sophisticated control. Therefore, insights from simple models for humans could be extended towards robot balance control. Robots have a myriad of sensors operating in different

units that need to be combined to estimate body state. Similarly, the human central nervous system must also contend with the integration of different sensors, each with their own dynamics. One such solution, as illustrated by my work, is to use an optimal estimator. This method will seek to minimize the error between predicted behavior and sensory measurements for a given set of noise parameters, which may be estimated from hardware specifications.

The one-legged balance research illustrated the importance of inertia and feedback in balance control. Given limited ankle torques, whether due to traditionally small robot feet or lack of actuators at the ankle for weight-savings, momentum from the available robotic limbs are important for indirectly moving the center of mass for balance. The importance of momentum was also demonstrated in the sagittal plane with sit-to-stand movement. Trunk momentum allowed seat-off to occur with the center of mass still posterior to the base of support and distributes knee and hip work. However this dynamic movement requires a brief moment of instability and therefore precise joint coordination. Lack of this coordination in existing robots necessitates quasi-static strategies such as maintaining the center of mass over the base of support or the use of static handholds. Finally, clearing the ground during swing is essential to avoiding falls for robots. The cost of ground clearance for robots may also be explained by a tradeoff between two costly measures. One stepping strategy could be to "stomp" on the ground, enabling adequate ground clearance and accurate sensory reading of footfall. This method might be preferred on a system with noisy or unsophisticated sensors. Another stepping strategy could be to skim the ground, less costly in lift work but has greater consequence in failure. Both of these are modulated by the accuracy of foot trajectory during swing, as any variability will incur costs from both strategies.

6.3 Future Research

Most model predictions are testable with human experimental data. For example, solutions to other chair rise behaviors can be recreated experimentally and compared against model results. This includes using strategies using only hip torque or only knee torque as well as momentum usage versus quasi-static movements. The ground clearance cost model also produced several testable predictions. For example, walking on uneven terrain necessitates greater foot lift. While several studies have shown this indirectly, such as through distance between a metatarsal marker at stance and lowest point in swing, true foot-to-ground distance is needed to accurately answer this question. Another prediction is that walking with no ground interference during swing may utilize less energy than for

preferred walking. This could be demonstrated with raised stepping stones which allow for swing without ground consequences yet incur minimal additional energetic cost for foot placement control. Two of these studies also involved balance control while standing. While basic mechanisms for sensory integration and limb coordination for balance are expected to remain the same during walking, new strategies or cross-coupling of sagittal and frontal plane dynamics may require further investigations.

BIBLIOGRAPHY

[1] A. L. Adkin, J. S. Frank, and M. S. Jog. Fear of falling and postural control in Parkinson's disease. *Mov. Disord.*, 18(5):496–502, May 2003.

[2] F. C. Anderson and M. G. Pandy. Dynamic optimization of human walking. *J Biomech Eng*, 123(5):381–390, Oct. 2001.

[3] R. S. Barrett, P. M. Mills, and R. K. Begg. A systematic review of the effect of ageing and falls history on minimum foot clearance characteristics during level walking. *Gait Posture*, 32(4):429–435, Oct. 2010.

[4] R. Begg, R. Best, L. Dell'Oro, and S. Taylor. Minimum foot clearance during walking: strategies for the minimisation of trip-related falls. *Gait Posture*, 25(2):191–198, Feb. 2007.

[5] R. K. Begg and W. A. Sparrow. Ageing effects on knee and ankle joint angles at key events and phases of the gait cycle. *J Med Eng Technol*, 30(6):382–389, Dec. 2006.

[6] K. Berg, S. Wood-Dauphine, J. Williams, and D. Gayton. Measuring balance in the elderly: preliminary development of an instrument. *Physiotherapy Canada*, 41(6):304–311, Nov. 1989.

[7] D. P. Bertsekas and J. N. Tsitsiklis. *Introduction to Probability*. Athena Scientific, Belmont, Mass., 1st edition edition, June 2002.

[8] R. W. Bohannon and K. M. Leary. Standing balance and function over the course of acute rehabilitation. *Arch Phys Med Rehabil*, 76(11):994–996, Nov. 1995.

[9] J. Borah, L. R. Young, and R. E. Curry. Optimal estimator model for human spatial orientation. *Ann. N. Y. Acad. Sci.*, 545:51–73, 1988.

[10] J. M. Brockway. Derivation of formulae used to calculate energy expenditure in man. *Hum Nutr Clin Nutr*, 41(6):463–471, Nov. 1987.

[11] A. E. Bryson. *Applied Linear Optimal Control*. Cambridge University Press, Sept. 2002.

[12] B. Cohen, V. Henn, T. Raphan, and D. Dennett. Velocity storage, nystagmus, and visual-vestibular interactions in humans. *Ann. N. Y. Acad. Sci.*, 374:421–433, 1981.

[13] T. H. Cruz and Y. Y. Dhaher. Impact of ankle-foot-orthosis on frontal plane behaviors post-stroke. *Gait Posture*, 30(3):312–316, Oct. 2009.

[14] A. R. De Asha and J. G. Buckley. The effects of walking speed on minimum toe clearance and on the temporal relationship between minimum clearance and peak swing-foot velocity in unilateral trans-tibial amputees. *Prosthet Orthot Int*, 39(2):120–125, Apr. 2015.

[15] J. C. Dean and A. D. Kuo. Elastic coupling of limb joints enables faster bipedal walking. *J R Soc Interface*, 6(35):561–573, June 2009.

[16] J. M. Donelan, R. Kram, and A. D. Kuo. Mechanical and metabolic determinants of the preferred step width in human walking. *Proc. Biol. Sci.*, 268(1480):1985–1992, Oct. 2001.

[17] J. M. Donelan, R. Kram, and A. D. Kuo. Simultaneous positive and negative external mechanical work in human walking. *J Biomech*, 35(1):117–124, Jan. 2002.

[18] A. G. Drusini, G. P. Eleazer, M. Caiazzo, E. Veronese, N. Carrara, C. Ranzato, F. Businaro, R. Boland, and D. Wieland. One-leg standing balance and functional status in an elderly community-dwelling population in northeast Italy. *Aging Clin Exp Res*, 14(1):42–46, Feb. 2002.

[19] C. Fernandez and J. M. Goldberg. Physiology of peripheral neurons innervating semicircular canals of the squirrel monkey. II. Response to sinusoidal stimulation and dynamics of peripheral vestibular system. *J. Neurophysiol.*, 34(4):661–675, July 1971.

[20] W. H. Gage, D. A. Winter, J. S. Frank, and A. L. Adkin. Kinematic and kinetic validity of the inverted pendulum model in quiet standing. *Gait Posture*, 19(2):124–132, Apr. 2004.

[21] D. H. Gates, J. M. Wilken, S. J. Scott, E. H. Sinitski, and J. B. Dingwell. Kinematic Strategies for Walking Across a Destabilizing Rock Surface. *Gait Posture*, 35(1):36–42, Jan. 2012.

[22] S. A. Glantz. *Primer of Biostatistics*. McGraw-Hill Medical, 4th edition, Apr. 2005.

[23] P. A. Goldie, T. M. Bach, and O. M. Evans. Force platform measures for evaluating postural control: reliability and validity. *Arch Phys Med Rehabil*, 70(7):510–517, July 1989.

[24] A. M. Green and D. E. Angelaki. Multisensory integration: resolving sensory ambiguities to build novel representations. *Curr. Opin. Neurobiol.*, 20(3):353–360, June 2010.

[25] S. E. Haggerty, A. R. Wu, K. H. Sienko, and A. D. Kuo. A shared neural integrator for human postural control. In Review.

[26] A. L. Hatton, J. C. Menant, S. R. Lord, J. C. M. Lo, and D. L. Sturnieks. The effect of lower limb muscle fatigue on obstacle negotiation during walking in older adults. *Gait Posture*, 37(4):506–510, Apr. 2013.

[27] A. L. Hof. The equations of motion for a standing human reveal three mechanisms for balance. *J Biomech*, 40(2):451–457, 2007.

[28] F. B. Horak. Postural orientation and equilibrium: what do we need to know about neural control of balance to prevent falls? *Age Ageing*, 35 Suppl 2:ii7–ii11, Sept. 2006.

[29] F. B. Horak and L. M. Nashner. Central programming of postural movements: adaptation to altered support-surface configurations. *J. Neurophysiol.*, 55(6):1369–1381, June 1986.

[30] M. A. Hughes, B. S. Myers, and M. L. Schenkman. The role of strength in rising from a chair in the functionally impaired elderly. *J Biomech*, 29(12):1509–1513, Dec. 1996.

[31] M. A. Hughes, D. K. Weiner, M. L. Schenkman, R. M. Long, and S. A. Studenski. Chair rise strategies in the elderly. *Clin Biomech (Bristol, Avon)*, 9(3):187–192, May 1994.

[32] E. Jonsson, A. Seiger, and H. Hirschfeld. One-leg stance in healthy young and elderly adults: a measure of postural steadiness? *Clin Biomech (Bristol, Avon)*, 19(7):688–694, Aug. 2004.

[33] E. R. Kandel, J. H. Schwartz, T. M. Jessell, S. A. Siegelbaum, and A. J. Hudspeth. *Principles of Neural Science*. McGraw-Hill Professional, New York, 5th edition, Oct. 2012.

[34] K. M. Kerr, J. A. White, D. A. Barr, and R. a. B. Mollan. Analysis of the sit-stand-sit movement cycle in normal subjects. *Clin Biomech (Bristol, Avon)*, 12(4):236–245, June 1997.

[35] D. C. Kerrigan, E. P. Frates, S. Rogan, and P. O. Riley. Hip hiking and circumduction: quantitative definitions. *Am J Phys Med Rehabil*, 79(3):247–252, June 2000.

[36] E. A. Keshner and R. V. Kenyon. The influence of an immersive virtual environment on the segmental organization of postural stabilizing responses. *J Vestib Res*, 10(4-5):207–219, 2000.

[37] T. Kiemel, K. S. Oie, and J. J. Jeka. Multisensory fusion and the stochastic structure of postural sway. *Biol Cybern*, 87(4):262–277, Oct. 2002.

[38] T. Kiemel, Y. Zhang, and J. J. Jeka. Visual flow is interpreted relative to multisegment postural control. *J Mot Behav*, 43(3):237–246, 2011.

[39] A. D. Kuo. An optimal control model for analyzing human postural balance. *IEEE Trans Biomed Eng*, 42(1):87–101, Jan. 1995.

[40] A. D. Kuo. An optimal state estimation model of sensory integration in human postural balance. *J Neural Eng*, 2(3):S235–249, Sept. 2005.

[41] S. G. Lisberger and W. T. Thach. The Cerebellum. In *Principles of Neural Science*, pages 960–981. McGraw-Hill Professional, New York, 5th edition, Oct. 2012.

[42] B. E. Maki, P. J. Holliday, and A. K. Topper. Fear of Falling and Postural Performance in the Elderly. *J Gerontol*, 46(4):M123–M131, July 1991.

[43] W. Mathiyakom, J. L. McNitt-Gray, P. Requejo, and K. Costa. Modifying center of mass trajectory during sit-to-stand tasks redistributes the mechanical demand across the lower extremity joints. *Clin Biomech (Bristol, Avon)*, 20(1):105–111, Jan. 2005.

[44] C. Maurer and R. J. Peterka. A new interpretation of spontaneous sway measures based on a simple model of human postural control. *J. Neurophysiol.*, 93(1):189–200, Jan. 2005.

[45] R. McNeill Alexander. Energetics and optimization of human walking and running: the 2000 Raymond Pearl memorial lecture. *Am. J. Hum. Biol.*, 14(5):641–648, Oct. 2002.

[46] P. G. Morasso and M. Schieppati. Can muscle stiffness alone stabilize upright standing? *J. Neurophysiol.*, 82(3):1622–1626, Sept. 1999.

[47] S. M. O'Connor and A. D. Kuo. Direction-dependent control of balance during walking and standing. *J. Neurophysiol.*, 102(3):1411–1419, Sept. 2009.

[48] E. Otten. Balancing on a narrow ridge: biomechanics and control. *Philos. Trans. R. Soc. Lond., B, Biol. Sci.*, 354(1385):869–875, May 1999.

[49] Y.-C. Pai, B. Naughton, R. Chang, and M. Rogers. Control of body centre of mass momentum during sit-to-stand among young and elderly adults. *Gait and Posture*, 2(2):109–116, 1994.

[50] M. G. Pandy, B. A. Garner, and F. C. Anderson. Optimal control of non-ballistic muscular movements: a constraint-based performance criterion for rising from a chair. *J Biomech Eng*, 117(1):15–26, Feb. 1995.

[51] S. Park, F. B. Horak, and A. D. Kuo. Postural feedback responses scale with biomechanical constraints in human standing. *Exp Brain Res*, 154(4):417–427, Feb. 2004.

[52] M. Paulin. A Kalman Filter Theory of the Cerebellum. In M. A. Arbib and S.-i. Amari, editors, *Dynamic Interactions in Neural Networks: Models and Data*, number 1 in Research Notes in Neural Computing, pages 239–259. Springer New York, 1989.

[53] M. G. Paulin. Evolution of the cerebellum as a neuronal machine for Bayesian state estimation. *J Neural Eng*, 2(3):S219–234, Sept. 2005.

[54] R. J. Peterka. Sensorimotor integration in human postural control. *J. Neurophysiol.*, 88(3):1097–1118, Sept. 2002.

[55] J. R. Rebula and A. D. Kuo. The Cost of Leg Forces in Bipedal Locomotion: A Simple Optimization Study. *PLoS One*, 10(2), Feb. 2015.

[56] P. O. Riley, M. L. Schenkman, R. W. Mann, and W. A. Hodge. Mechanics of a constrained chair-rise. *J Biomech*, 24(1):77–85, 1991.

[57] D. A. Robinson. Linear addition of optokinetic and vestibular signals in the vestibular nucleus. *Exp Brain Res*, 30(2-3):447–450, Nov. 1977.

[58] D. A. Robinson. Vestibular and optokinetic symbiosis: An example of explaining by modeling. In *Control of Gaze by Brain Stem Neurons*, pages 49–58. Elsevier, Amsterdam, NY, 1 edition, 1977.

[59] D. M. Scarborough, C. A. McGibbon, and D. E. Krebs. Chair rise strategies in older adults with functional limitations. *J Rehabil Res Dev*, 44(1):33–42, 2007.

[60] M. Schenkman, R. A. Berger, P. O. Riley, R. W. Mann, and W. A. Hodge. Whole-body movements during rising to standing from sitting. *Phys Ther*, 70(10):638–648; discussion 648–651, Oct. 1990.

[61] A. B. Schultz, N. B. Alexander, and J. A. Ashton-Miller. Biomechanical analyses of rising from a chair. *J Biomech*, 25(12):1383–1391, Dec. 1992.

[62] B. W. Schulz. Minimum toe clearance adaptations to floor surface irregularity and gait speed. *J Biomech*, 44(7):1277–1284, Apr. 2011.

[63] A. Shumway-Cook and M. H. Woollacott. *Motor control: theory and practical applications*. Number x, 614 p. Lippincott Williams & Wilkins, Philadelphia, 2001.

[64] M. Srinivasan and A. Ruina. Computer optimization of a minimal biped model discovers walking and running. *Nature*, 439(7072):72–75, Jan. 2006.

[65] S. Tanahashi, H. Ujike, R. Kozawa, and K. Ukai. Effects of visually simulated roll motion on vection and postural stabilization. *J Neuroeng Rehabil*, 4:39, 2007.

[66] M. E. Tinetti. Performance-oriented assessment of mobility problems in elderly patients. *J Am Geriatr Soc*, 34(2):119–126, Feb. 1986.

[67] W. N. van Asten, C. C. Gielen, and J. J. van der Gon. Postural movements induced by rotations of visual scenes. *J Opt Soc Am A*, 5(10):1781–1789, Oct. 1988.

[68] H. van der Kooij, R. Jacobs, B. Koopman, and H. Grootenboer. A multisensory integration model of human stance control. *Biol Cybern*, 80(5):299–308, May 1999.

[69] B. J. Vellas, S. J. Wayne, L. Romero, R. N. Baumgartner, L. Z. Rubenstein, and P. J. Garry. One-leg balance is an important predictor of injurious falls in older persons. *J Am Geriatr Soc*, 45(6):735–738, June 1997.

[70] A. S. Voloshina, A. D. Kuo, M. A. Daley, and D. P. Ferris. Biomechanics and energetics of walking on uneven terrain. *J. Exp. Biol.*, 216(Pt 21):3963–3970, Nov. 2013.

[71] D. Winter. Human balance and posture control during standing and walking. *Gait & Posture*, 3(4):193–214, Dec. 1995.

[72] D. Winter. *Biomechanics and Motor Control of Human Movement*. Wiley, Aug. 2004.

[73] D. A. Winter. Foot trajectory in human gait: a precise and multifactorial motor control task. *Phys Ther*, 72(1):45–53; discussion 54–56, Jan. 1992.

[74] J. M. Winters and A. H. Seif-Naraghi. Strategies for goal-directed fast movements are byproducts of satisfying performance criteria. *Behavioral and Brain Sciences*, 14(02):357–359, June 1991.

[75] L. R. Young. Perception of the Body in Space: Mechanisms. In *Comprehensive Physiology*. John Wiley & Sons, Inc., 2011.

[76] K. E. Zelik and A. D. Kuo. Human walking isn't all hard work: evidence of soft tissue contributions to energy dissipation and return. *J. Exp. Biol.*, 213(Pt 24):4257–4264, Dec. 2010.